WBD Studies of AKR: Coordinated Observations of Aurora and the SAKR – Ion Hole Connection

R. L. Mutel

University of Iowa

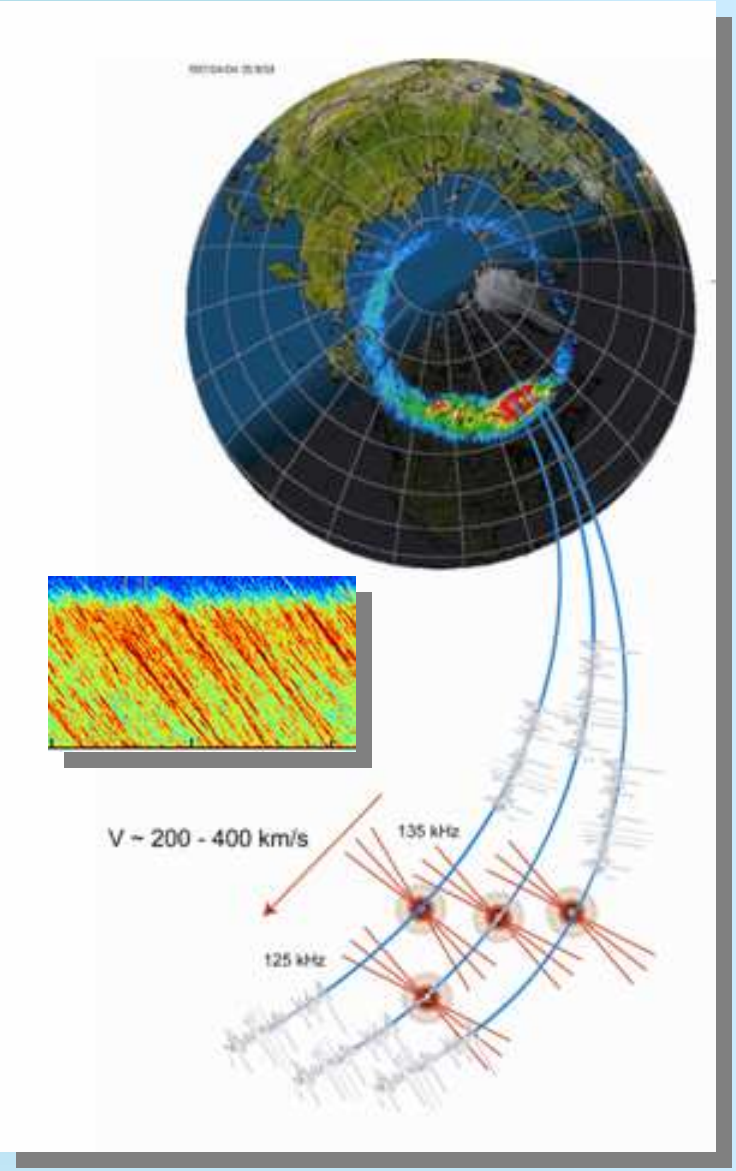

Outline

- Summary of AKR Properties
- AKR-Auroral Studies
  - VLBI technique, uncertainties
  - AKR – Auroral zone source location studies
  - Example: 8 June 2004
- Striated AKR SAKR – Ion ‘holes’
  - Summary of SAKR properties
  - Comparison with Ion Solitary Structures
  - Do Ion solitary structures trigger SAKR?

Characteristics of Terrestrial Auroral Kilometric Radiation

- Detected 25% - 50% of time
  - •Seasonal dependence: more frequent in winter
- Strongly associated w. geomagnetic activity, aurora
- Frequency 50 KHz – 1 MHz
  - Satellite detection only (ionosphere blocks terrestrial reception)
- Generation mechanism: e^- cyclotron maser
  - Requires e- distribution function: $\frac{\partial f}{\partial V_\perp} > 0$
- Freq-time spectra show complex structure
  - Broadband drifting bursts last ~hrs
  - Fine structure – narrowband, drifting timescale ~ seconds
  - **SAKR (Striated AKR)**
  - **Negative freq. drift => V~100-200 km/s**
  - **Assoc w. solitary structures? (focus of this talk)**

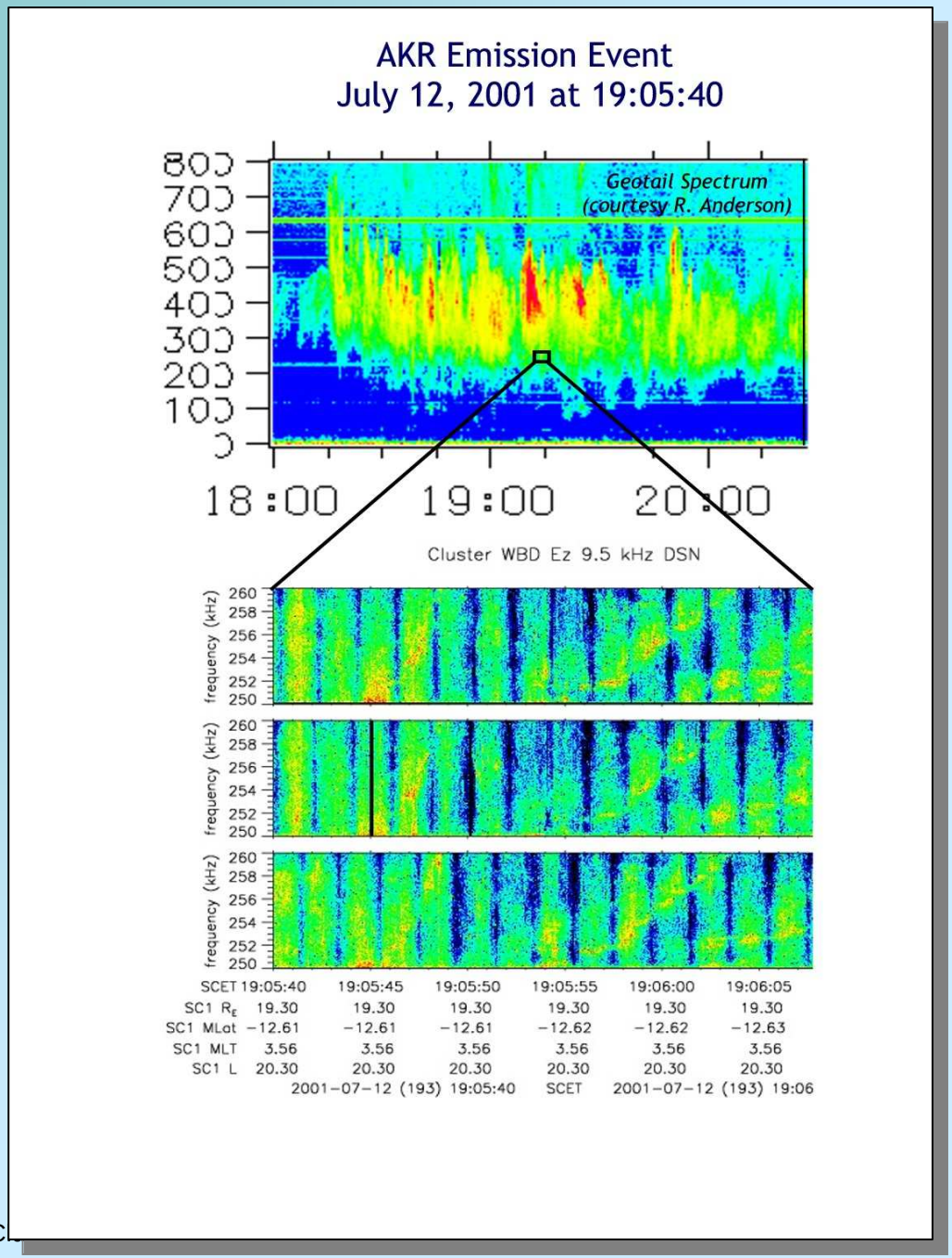

AKR Source region:

FAST Observations of AKR Source Region (Ergun et al. Ap. J. **538**, 456)

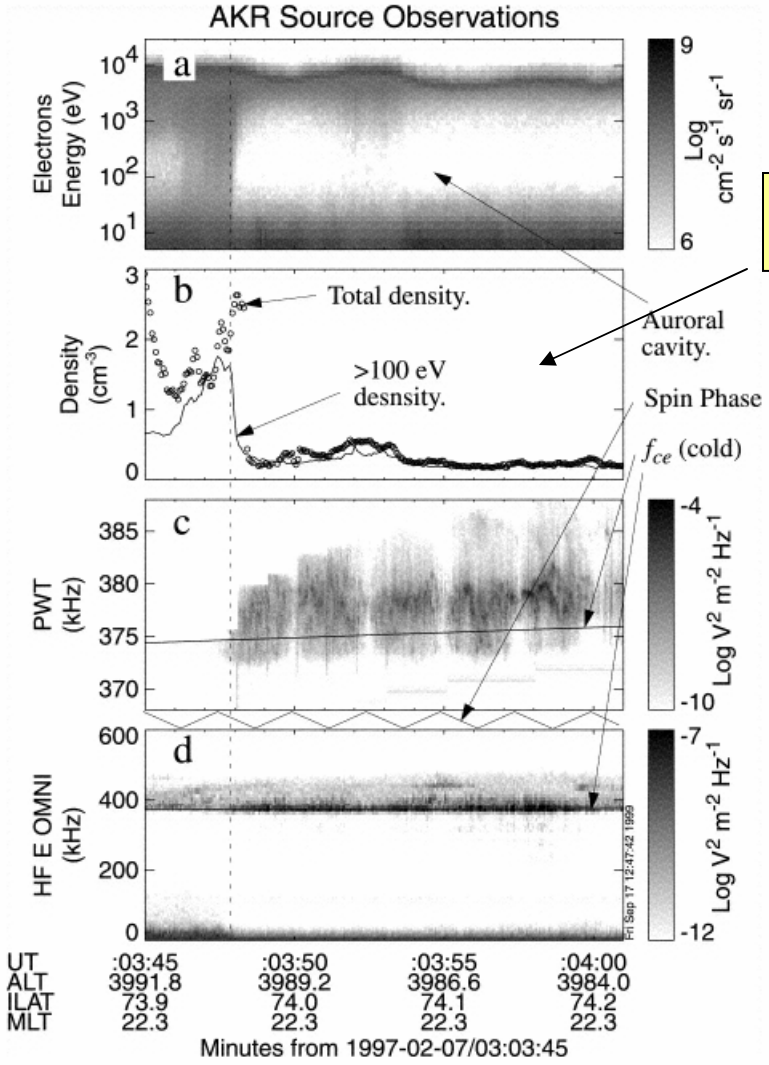

Note e$^-$ depletion in auroral cavity

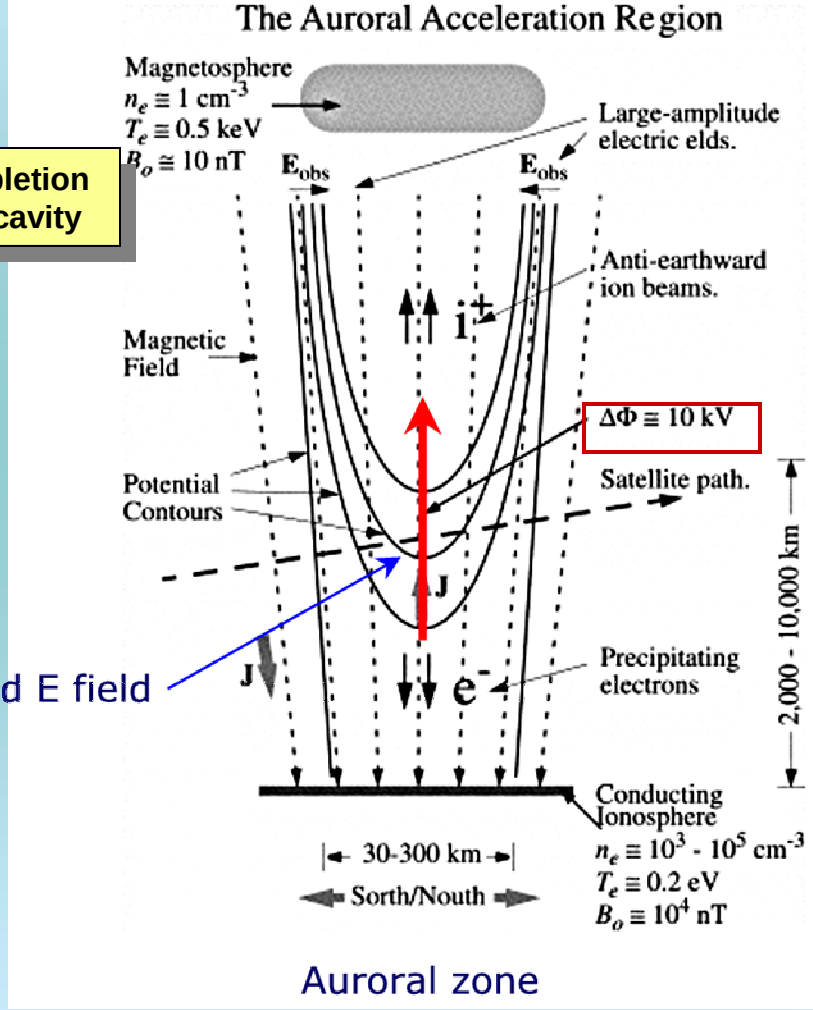

Upward E field

Auroral zone

FAST Observations of AKR Source Region (Ergun et al. Ap. J. **538**, 456)

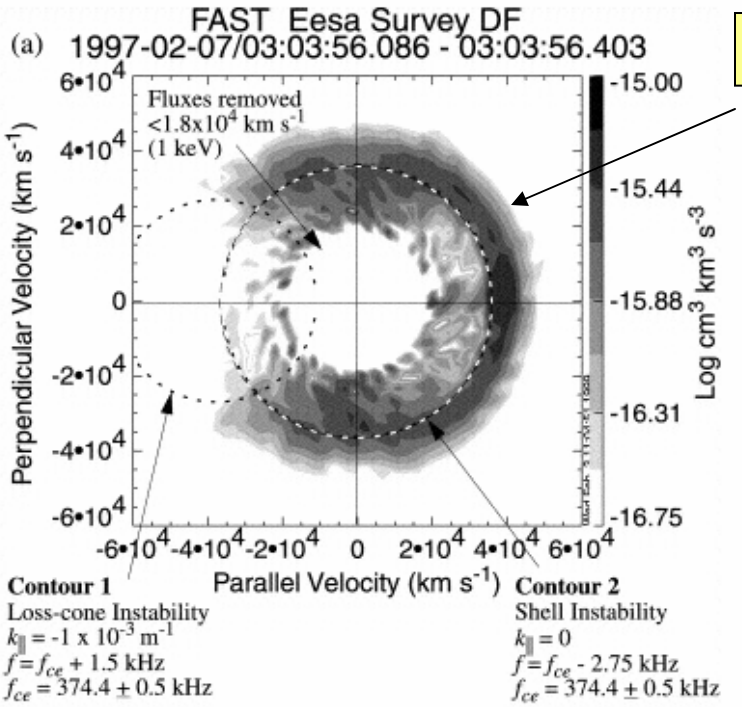

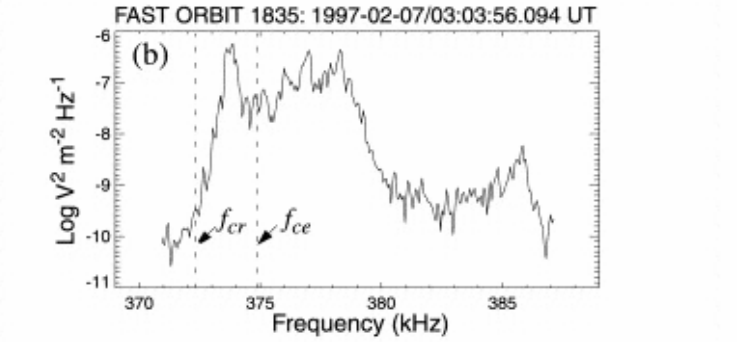

Shell instability

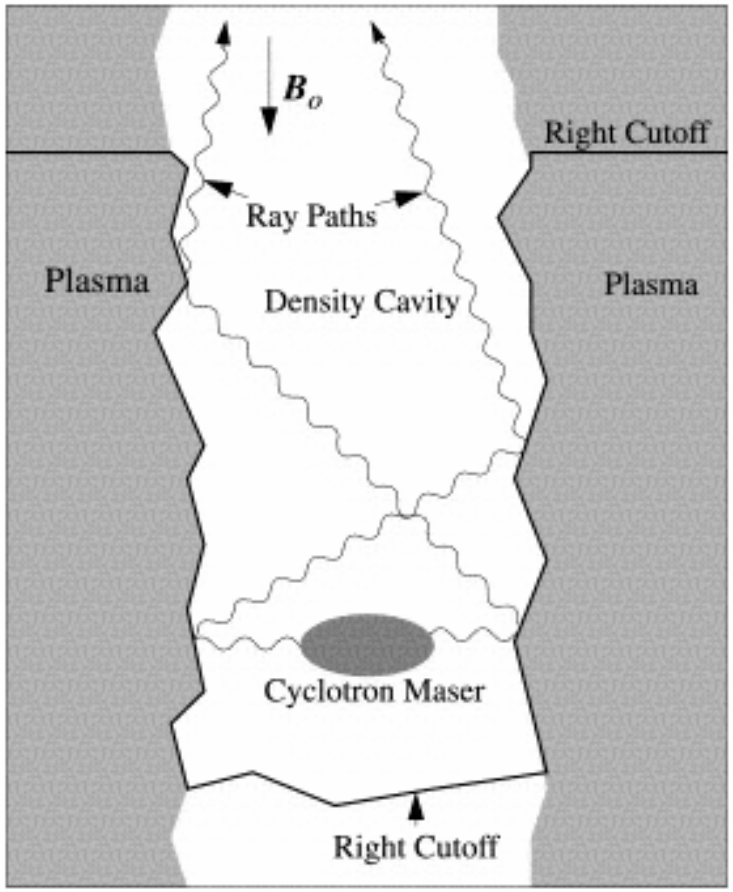

Closed cycle system connecting AKR with auroral region

- Free energy source for AKR consists of accelerated primary electrons (downward) and mirrored electrons (upward) with substantial $V_{\perp}$

- Mirroring (& turbulence) scatters beamed ($V_{||}$) electrons in velocity space

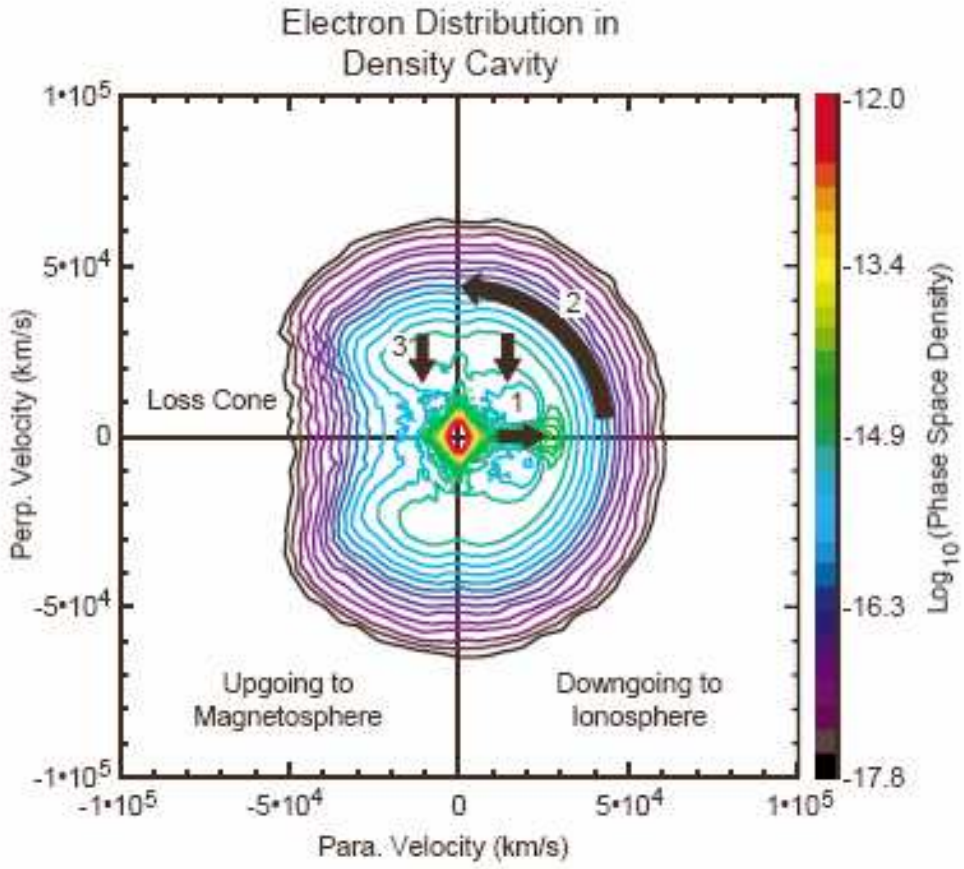

Fig. 6. Cartoon showing the energy flow within the AKR source region.

From Strangeway et al. 2000

Sample AKR dynamical spectra showing effect of angular beaming (see Christopher et al. poster Thursday)

SC1-SC4 angular sep'n ~14º

SC1-SC4 angular sep'n ~30º

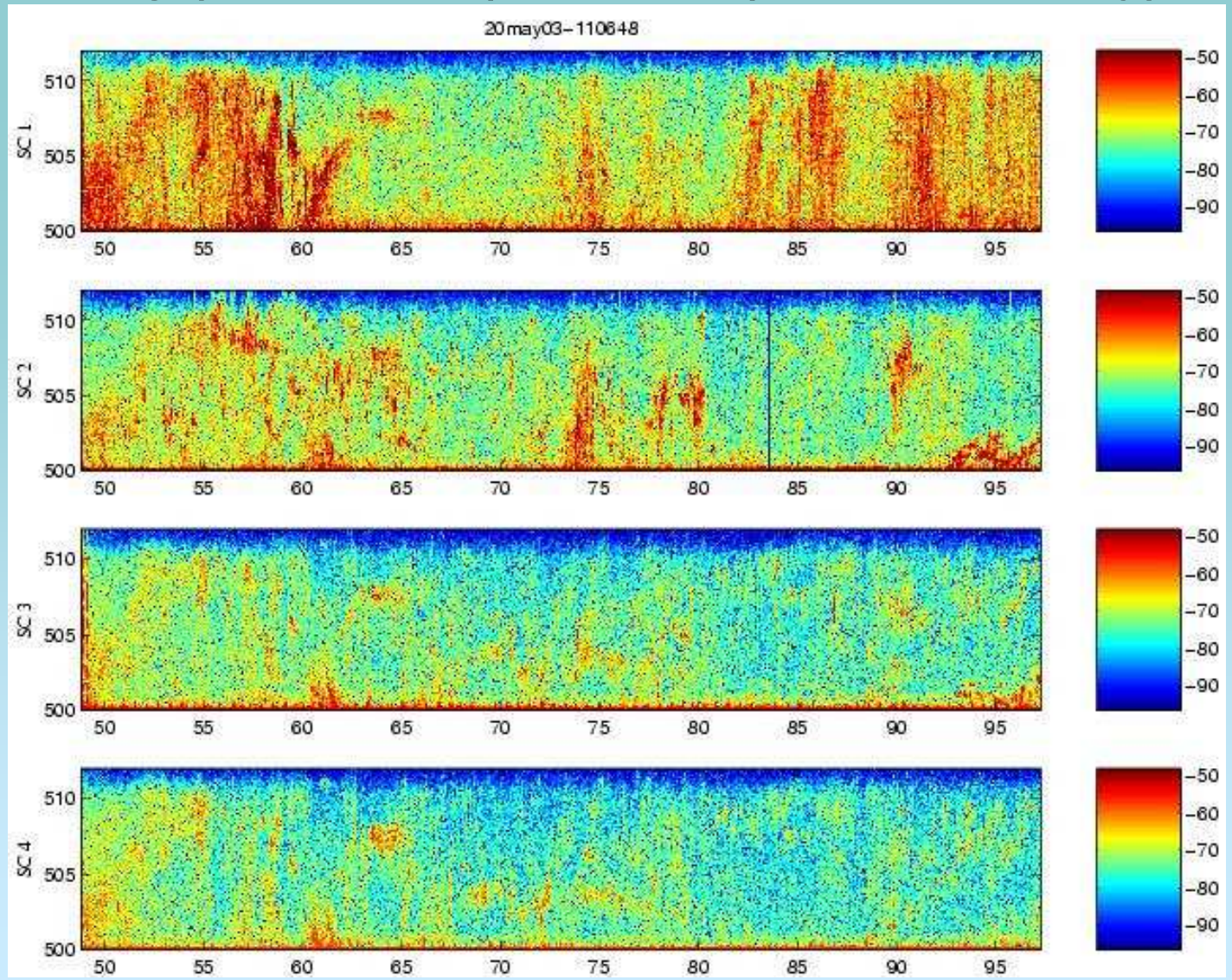

VLBI Source Location Algorithm: Differential delay measurement

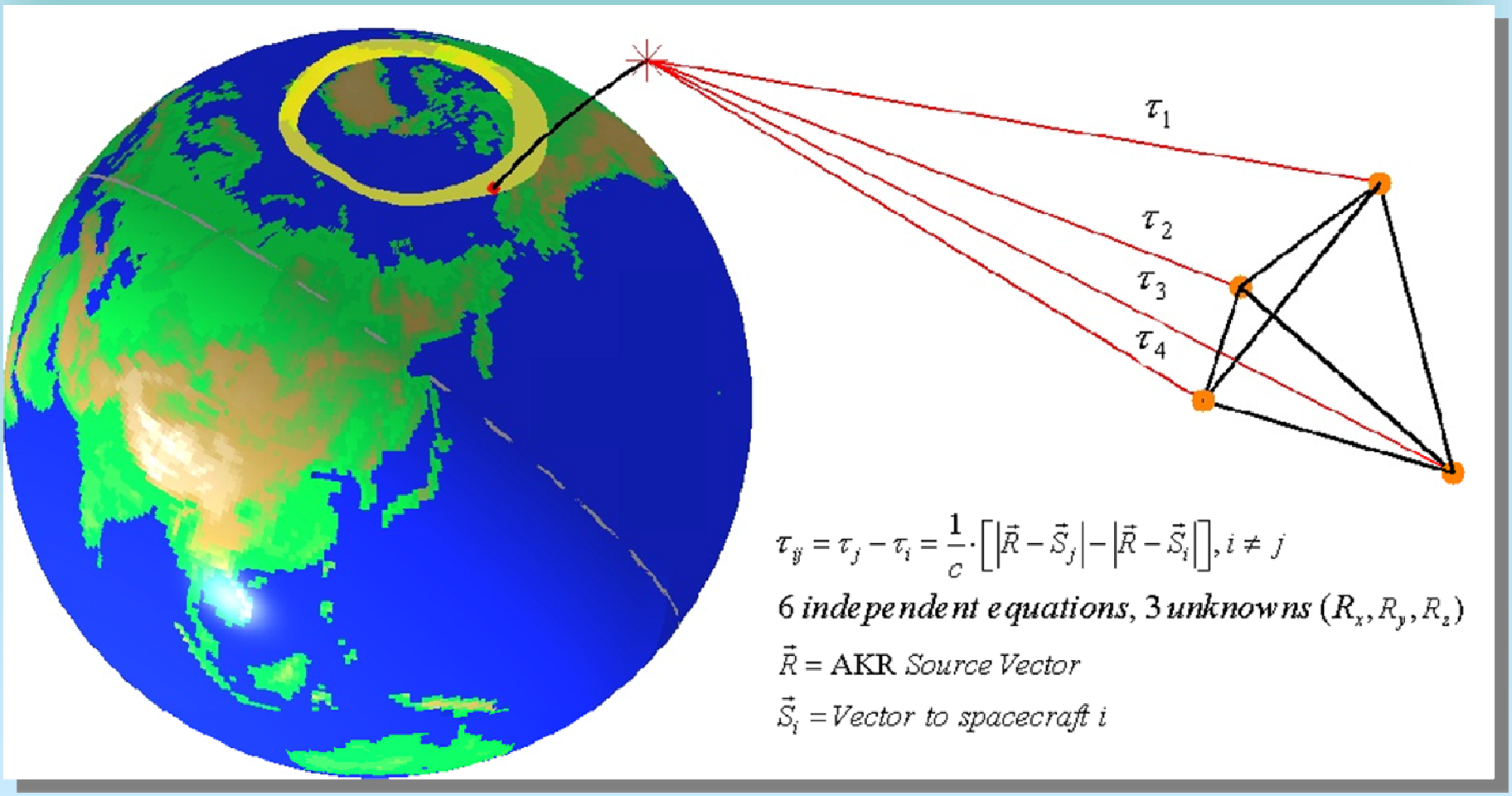

$$\tau_{ij} = \tau_j - \tau_i = \frac{1}{c} \cdot \left[\left| \vec{R} - \vec{S}_j \right| - \left| \vec{R} - \vec{S}_i \right| \right], i \neq j$$

6 *independent equations*, 3 *unknowns* (R_x, R_y, R_z)

$\vec{R}$ = AKR *Source Vector*

$\vec{S}_i$ = *Vector to spacecraft i*

Sample Dynamic Spectrum, Waveform and Cross-correlation

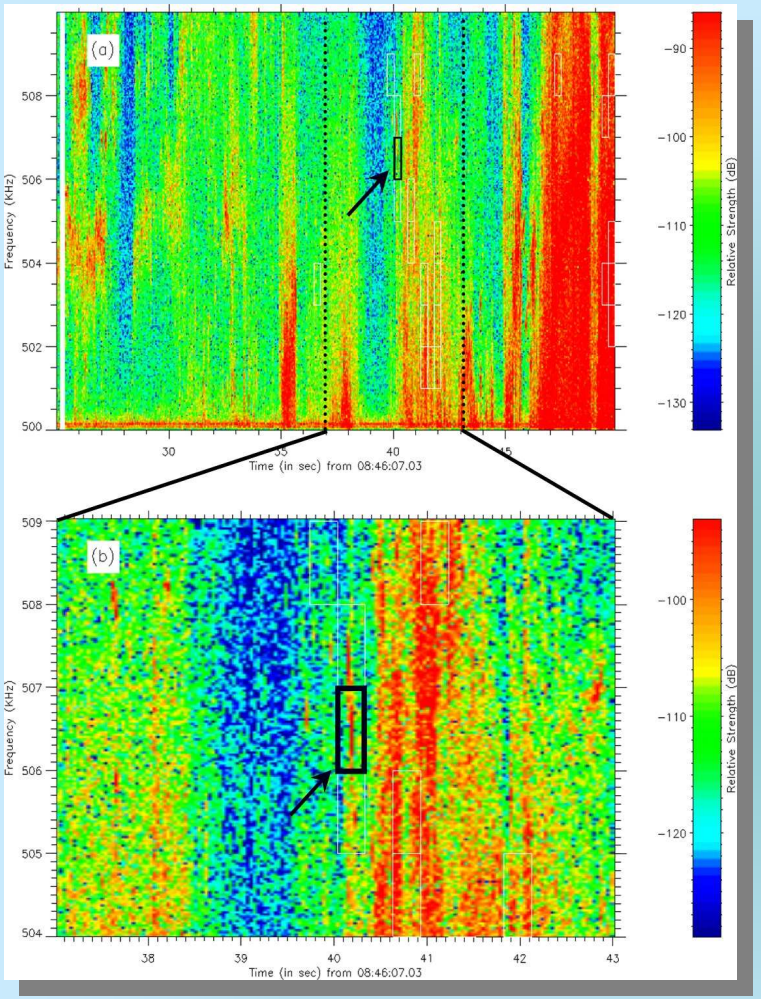

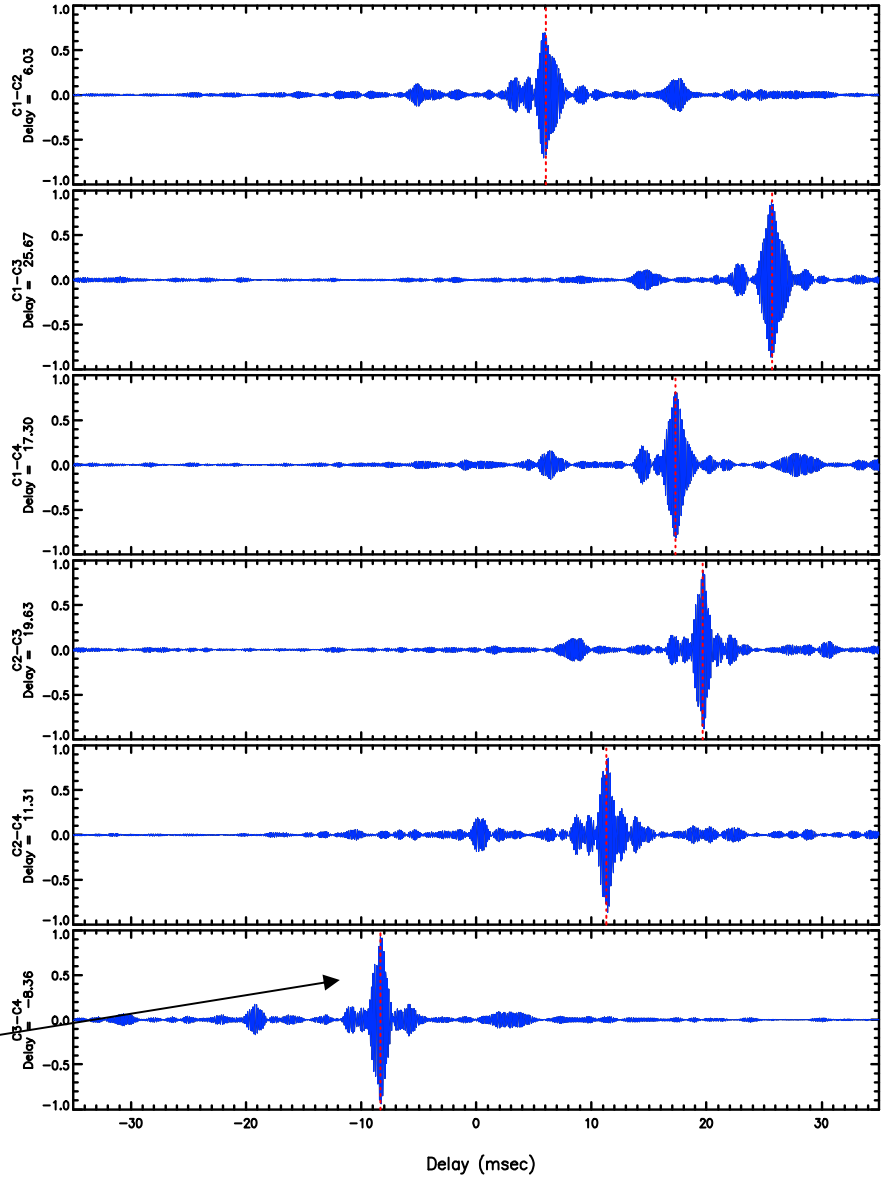

Peak is fit with Gaussian,
delay uncertainty $\Delta\tau \sim 0.3$ ms

Fly-through of AKR positions

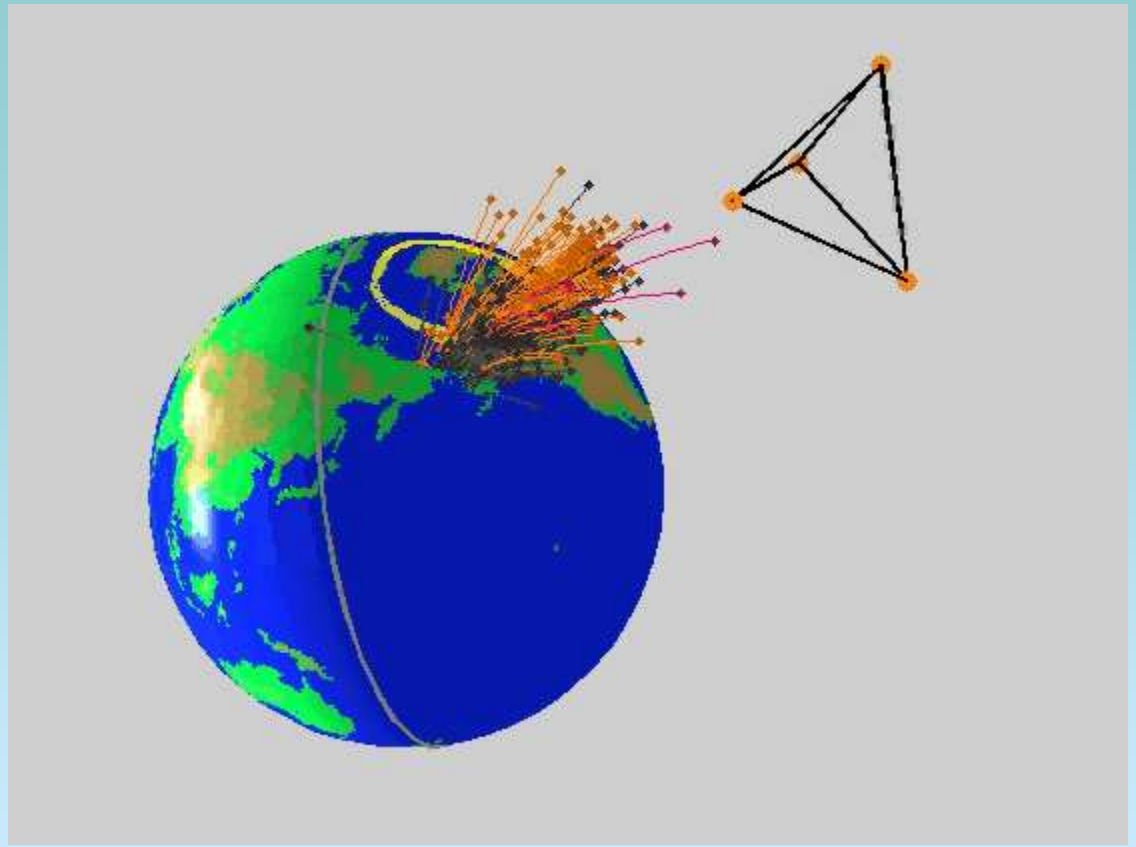

VLBI position uncertainty calculation

Delay uncertainties in plane ⊥ and parallel to line of sight:

$$\delta\tau = \frac{1}{c}\cdot\left\{\left[z^2+\left(\frac{B}{2}+\delta x_{\perp}\right)^2\right]^{\frac{1}{2}}-\left[z^2+\left(\frac{B}{2}-\delta x_{\perp}\right)^2\right]^{\frac{1}{2}}\right\}$$

Typical uncertainty in ⊥ plane:

$$\delta x_{\perp} \approx \left(\frac{z}{B}\right)\cdot c\delta\tau \approx 500\ km$$

Typical uncertainty in $x_{\parallel}$ plane:

$$\delta x_{\parallel} \approx 2\left(\frac{z}{B}\right)^2\cdot c\delta\tau \approx 5{,}000\ km$$

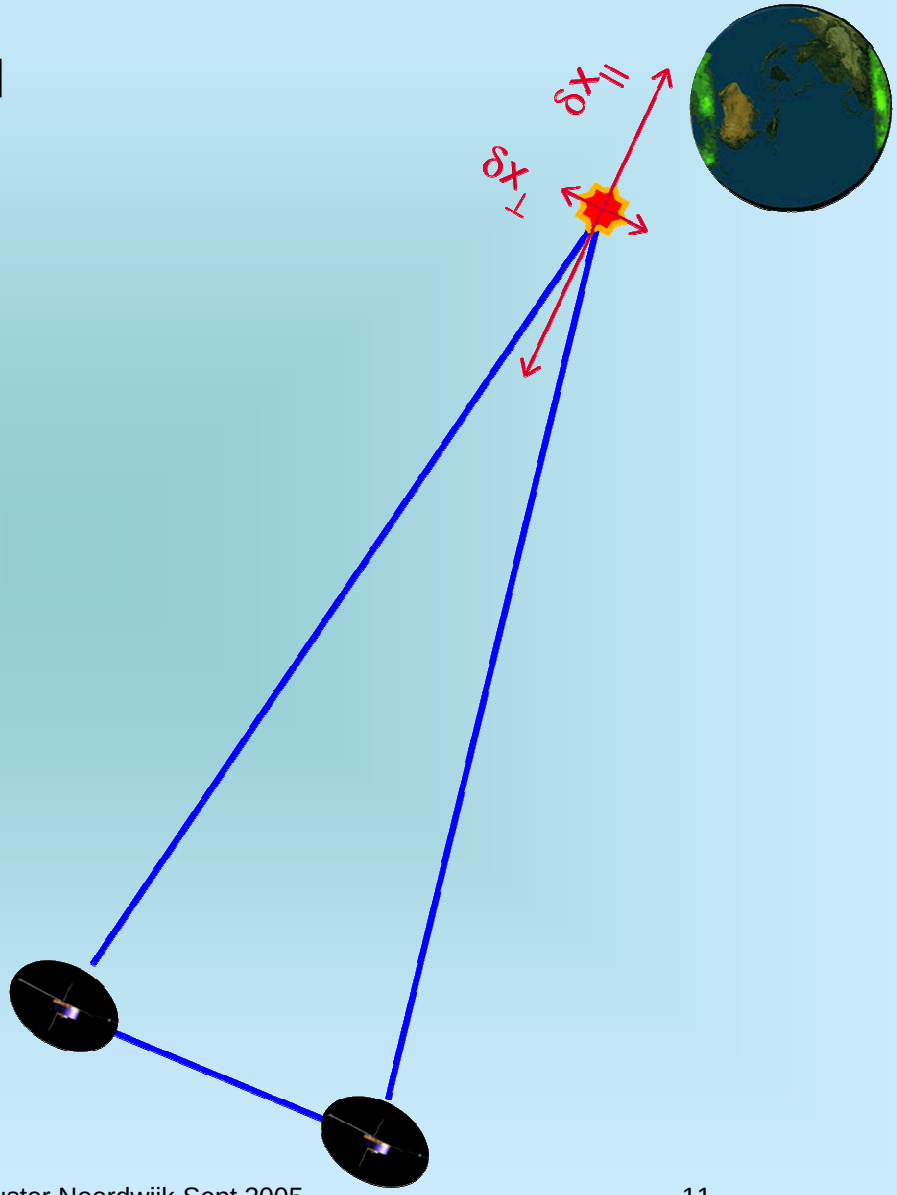

Movies of temporal behavior of Aurora, AKR

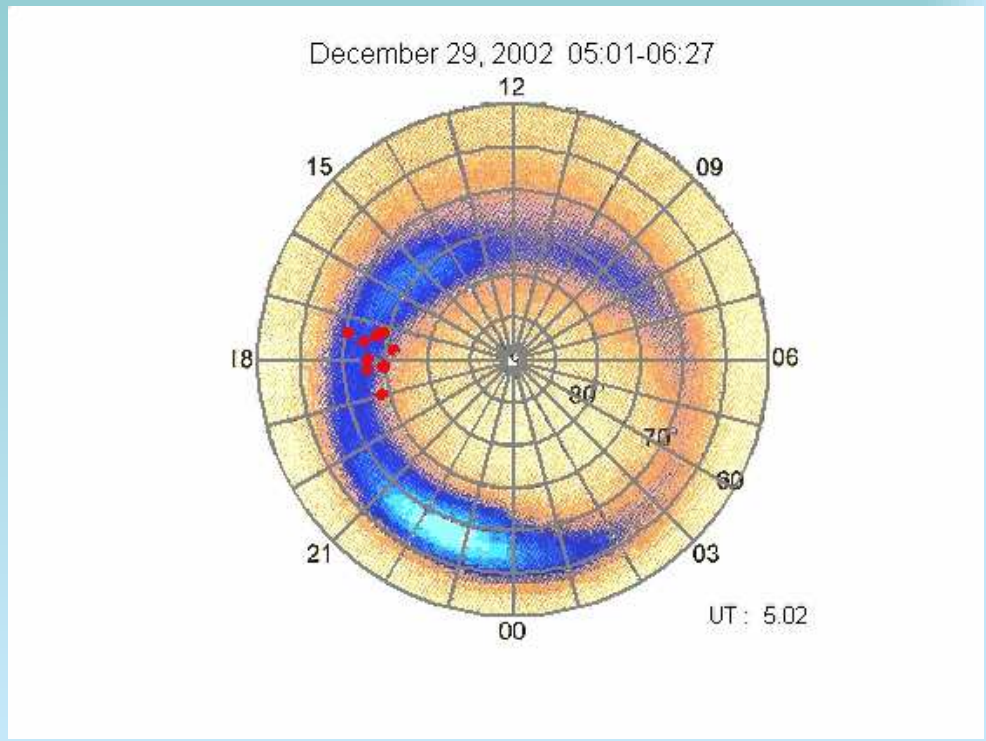

Case 1: Electron Acceleration Region Above AKR Source Region

Nominal Predictions:

- High Correlation Between AKR Source and Auroral Bright Features on Same Magnetic Field line
- Assumes electron precipitation continues to auroral region [suitable f(v)]
- But upward mirrored elecgtrons can still contribute

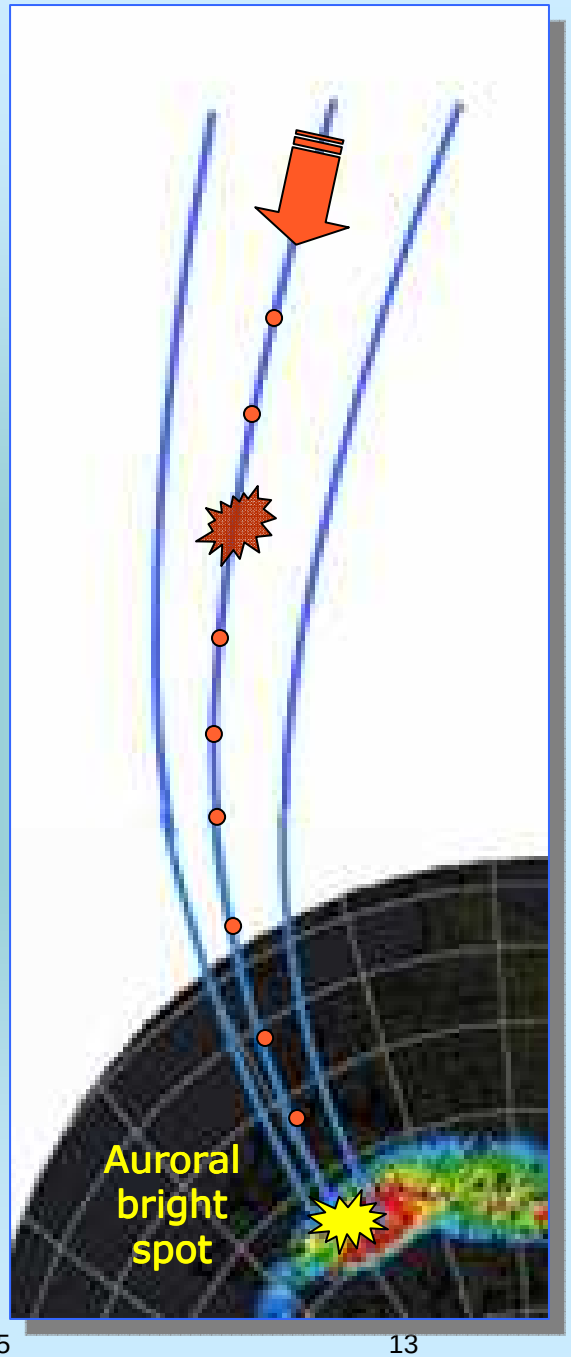

Case 2: Electron Acceleration Region Below AKR Source Region

Nominal Predictions:

- Low Correlation Between AKR Source and Auroral Bright Features on Same Magnetic Field line
- If AKR emission, sources not on same field line
- Possibility that upward scattered electrons could trigger AKR

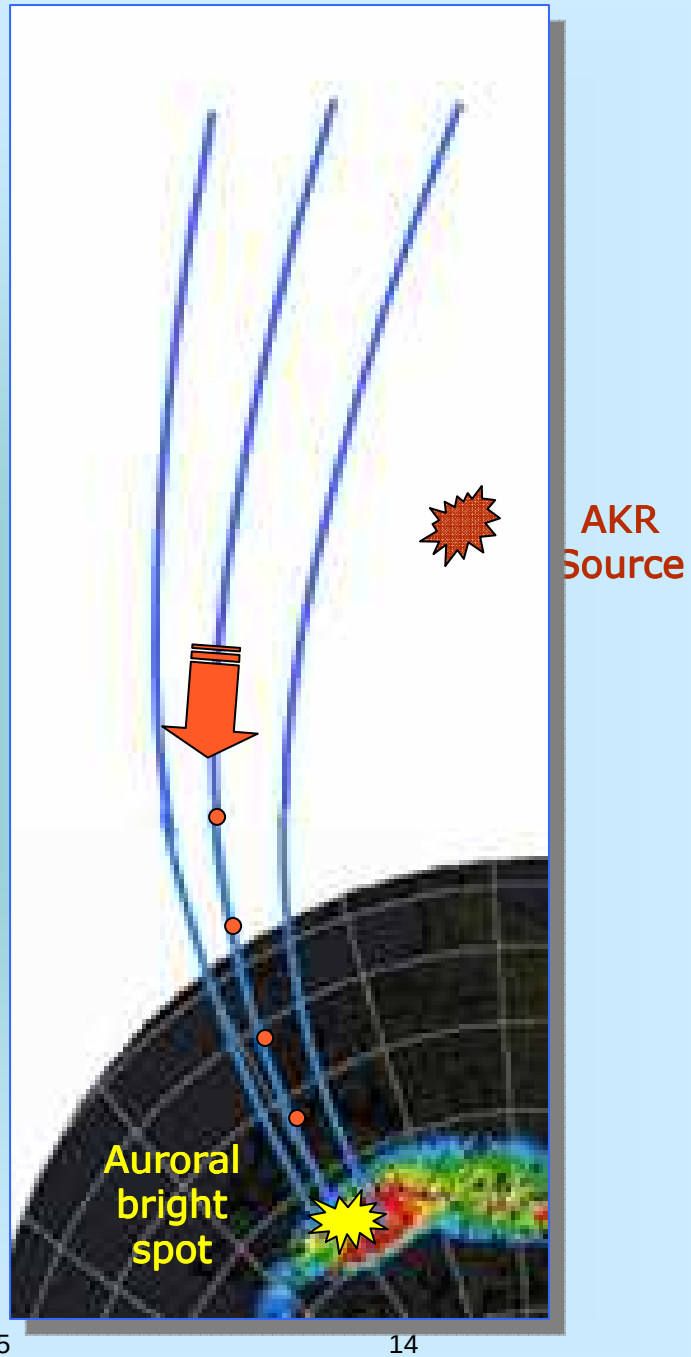

IMAGE Auroral Images
8 June 2004 11:30 – 11:49 UT

AKR Source Locations
8 June 2004 (11:13 – 11:51 UT)

Both movies

Striated AKR (SAKR)

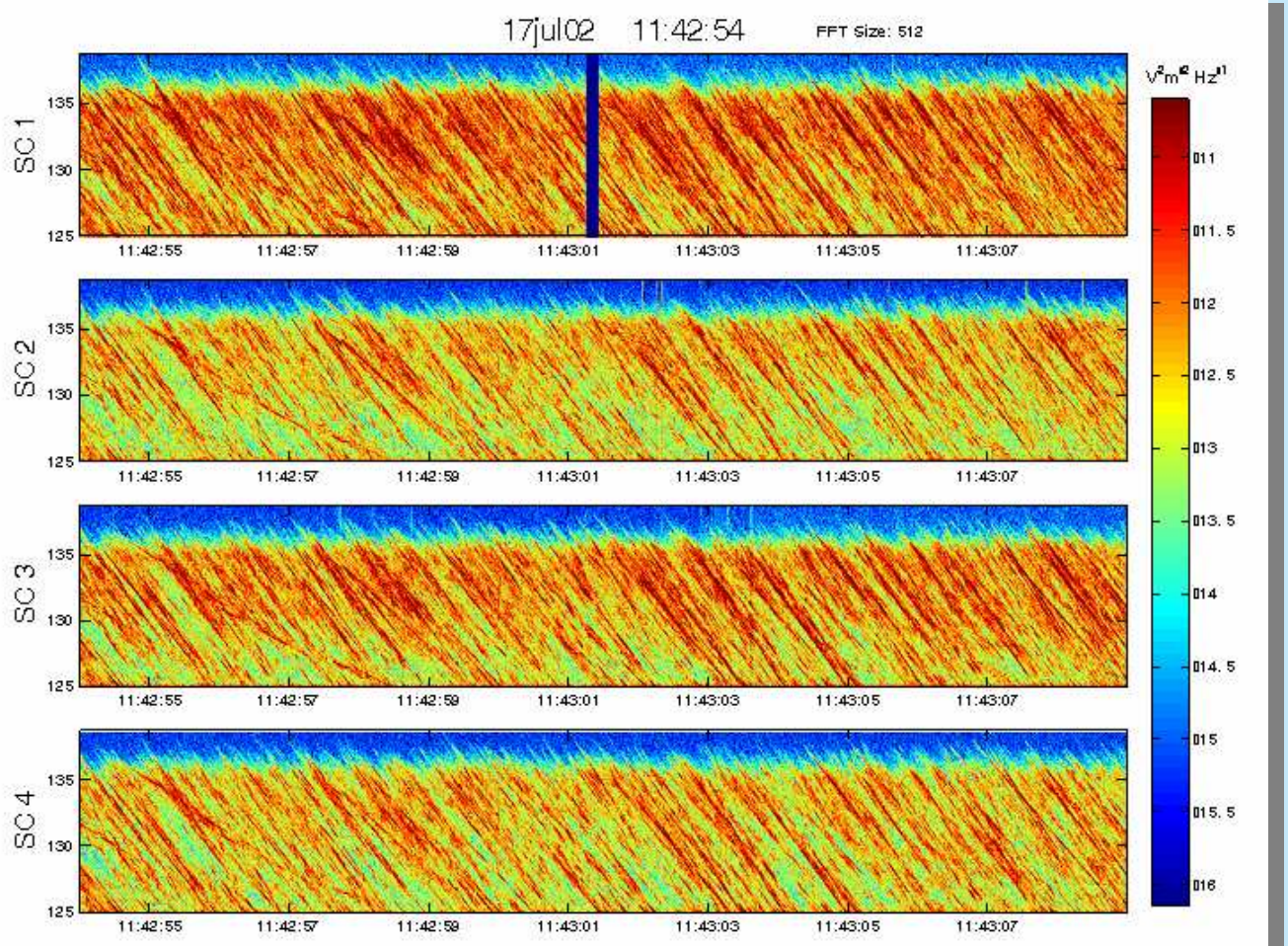

Figure 1. Example dynamical spectra of striated AKR bursts observed from 11:42:54 to 11:43:09 UT on 17 July 2002 on four Cluster spacecraft The spacecraft were located at geocentric distances between 10.6 (SC1) and 11.7 (SC3) Earth radii and magnetic latitude -55° (SC4) to -65° (SC1). The absence of emission above 135 kHz is due to filter roll-off in the receivers.

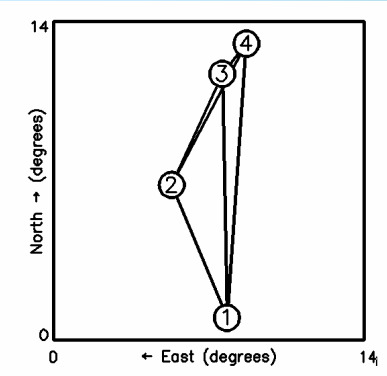

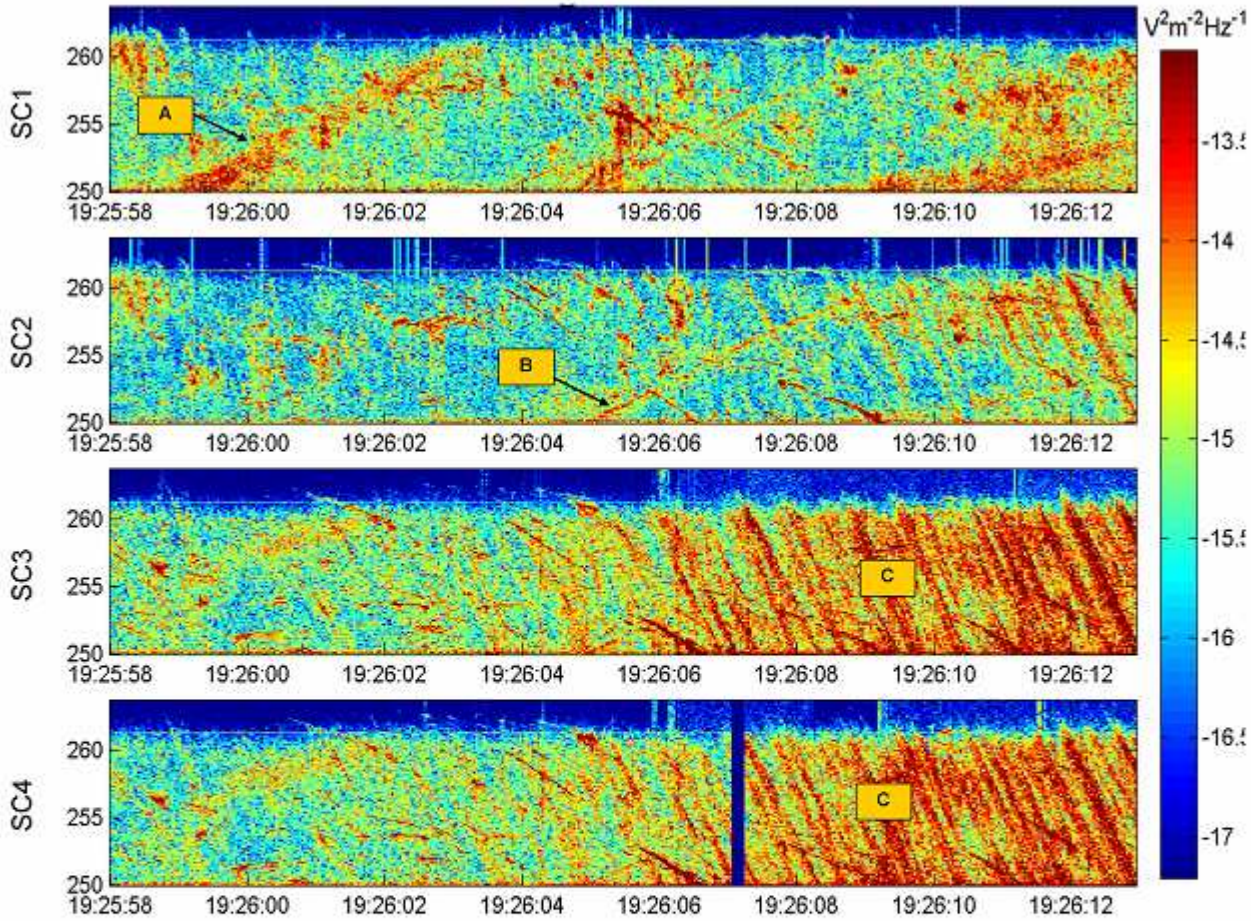

Figure xxx. Dynamical spectrum of a variety of AKR bursts observed on August 31, 2002 at 19:25:58 – 19:26:12 UT in the 250 kHz band. The Cluster spacecraft were located over the southern magnetic pole at geocentric distance between 8.6 and 9.7 Re and geomagnetic latitudes -79° to -86°. The angular separation of the Cluster constellation as viewed from 2 Re above the southern geomagnetic pole (assumed to be near the source location) is shown on figure xx. Note the relatively wideband (~1 kHz) positively drifting AKR burst labeled A, the narrowband isolated positively drifting feature labeled B, and the characteristic series of descending, narrowband striated bursts labeled C. The striated bursts are detected strongly only on spacecraft SC3 and SC4 (angular separation ~1.5°), illustrating the small angular size of the emission beam.

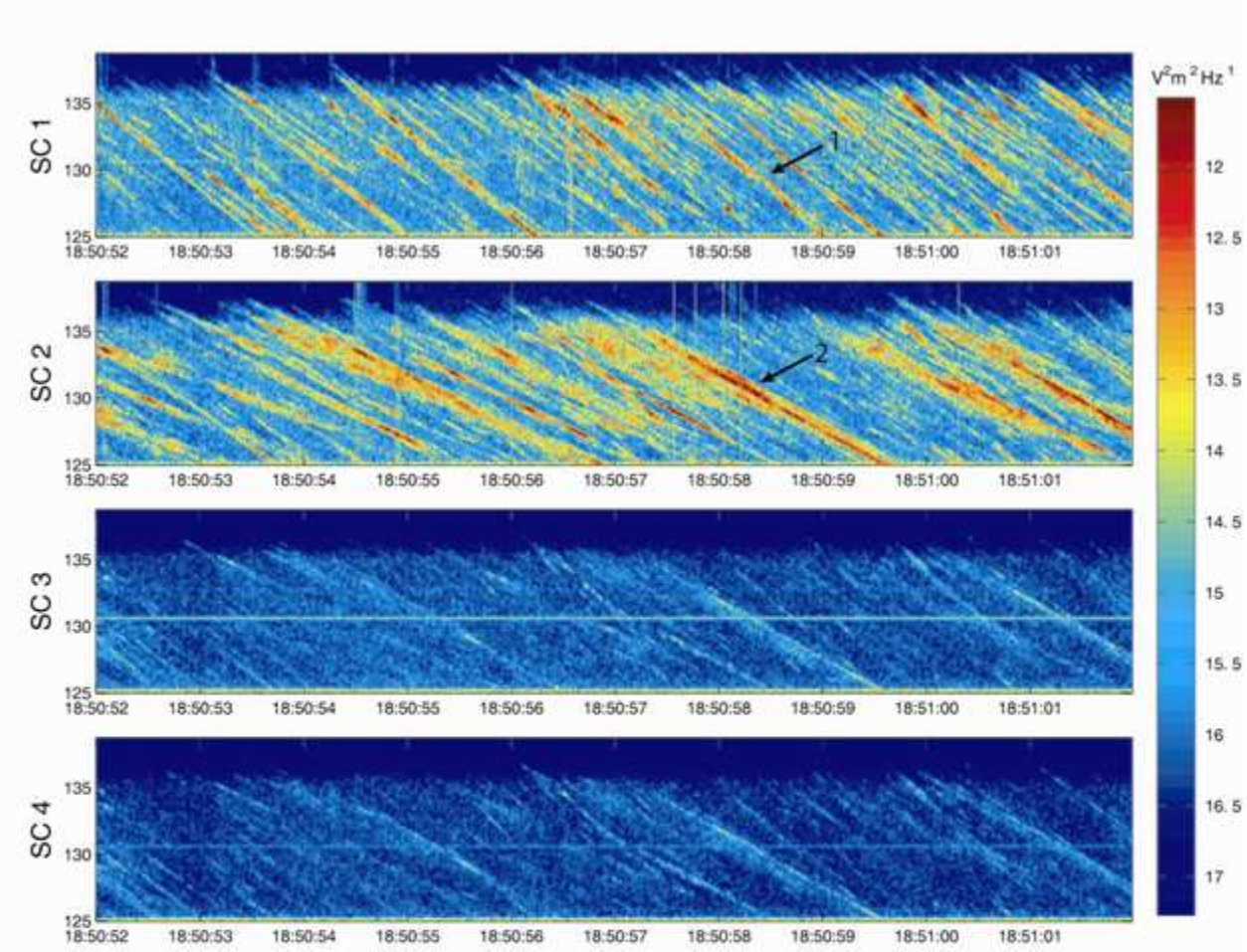

Figure xxx. Frequency-time spectra of drifting striated AKR bursts observed on 31 August 2002 between 18:50:52 UT and 18:51:02 UT. The bursts were observed by the WBD instrument in the 1250137 KHz band on four Cluster spacecraft (SC1- SC4) located at geocentric distances of 8.8Re (SC1) to 9.4 Re (SC4). The projected angular separation of the spacecraft as seen from a point 2Re above the south magnetic pole, is shown in figure xx. Note that SC1's spectrum is dominated by striated bursts (labeled 1) with slope df/dt ~ -6.4 kHz/s, while the dominant bursts observed at SC2 (labeled 2) have slope df/dt ~ -3.5 kHz/sec.

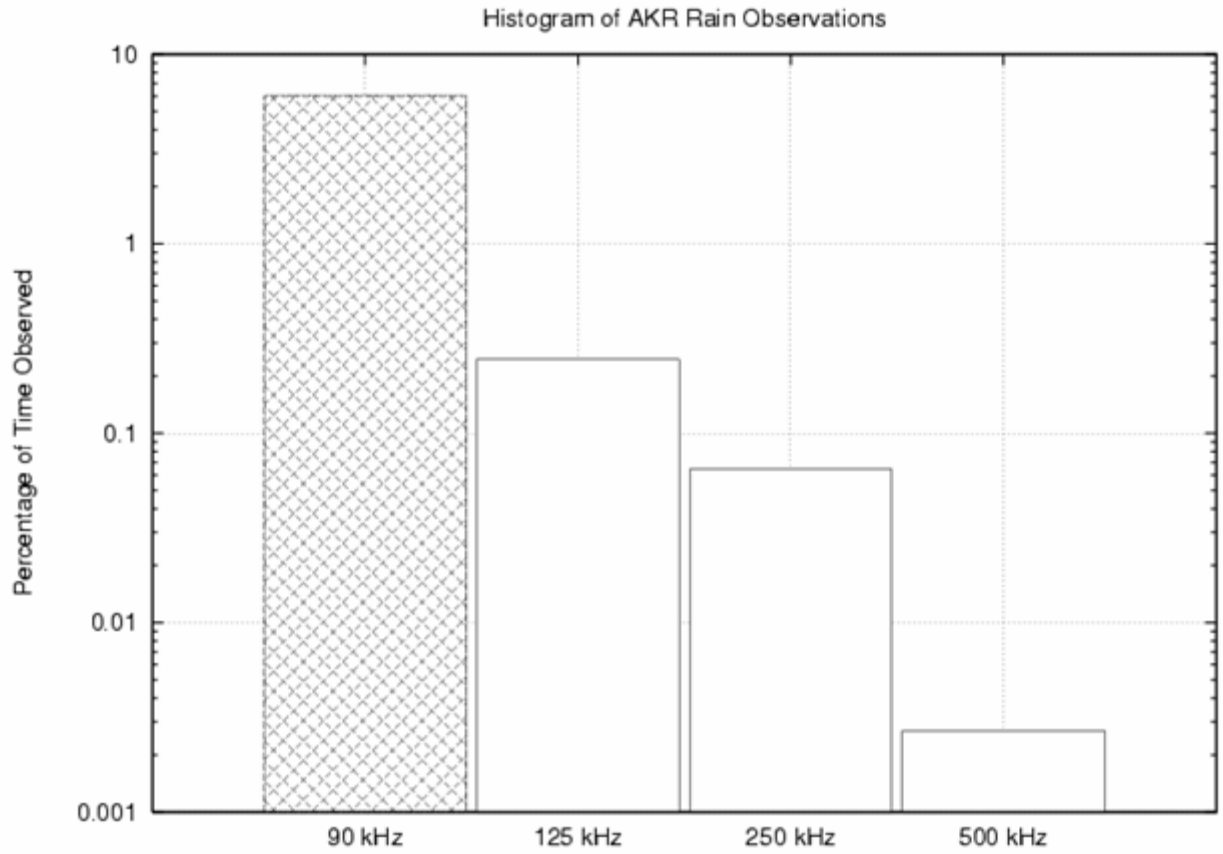

Figure xxx. Probability of detection of striated AKR bursts in a randomly chosen 52 sec time interval for observations in the 125, 250, and 500 KHz bands at a given spacecraft location. Note that within each 52 sec time interval, striated AKR is typically detected for a fraction of the total 52 sec interval, so these probabilities are an upper limit to the probability of detection for short sampling times. We have also included the probability of detection as reported by *Menietti et al* [2000] in the frequency band 0-90 kHz (shaded bar).

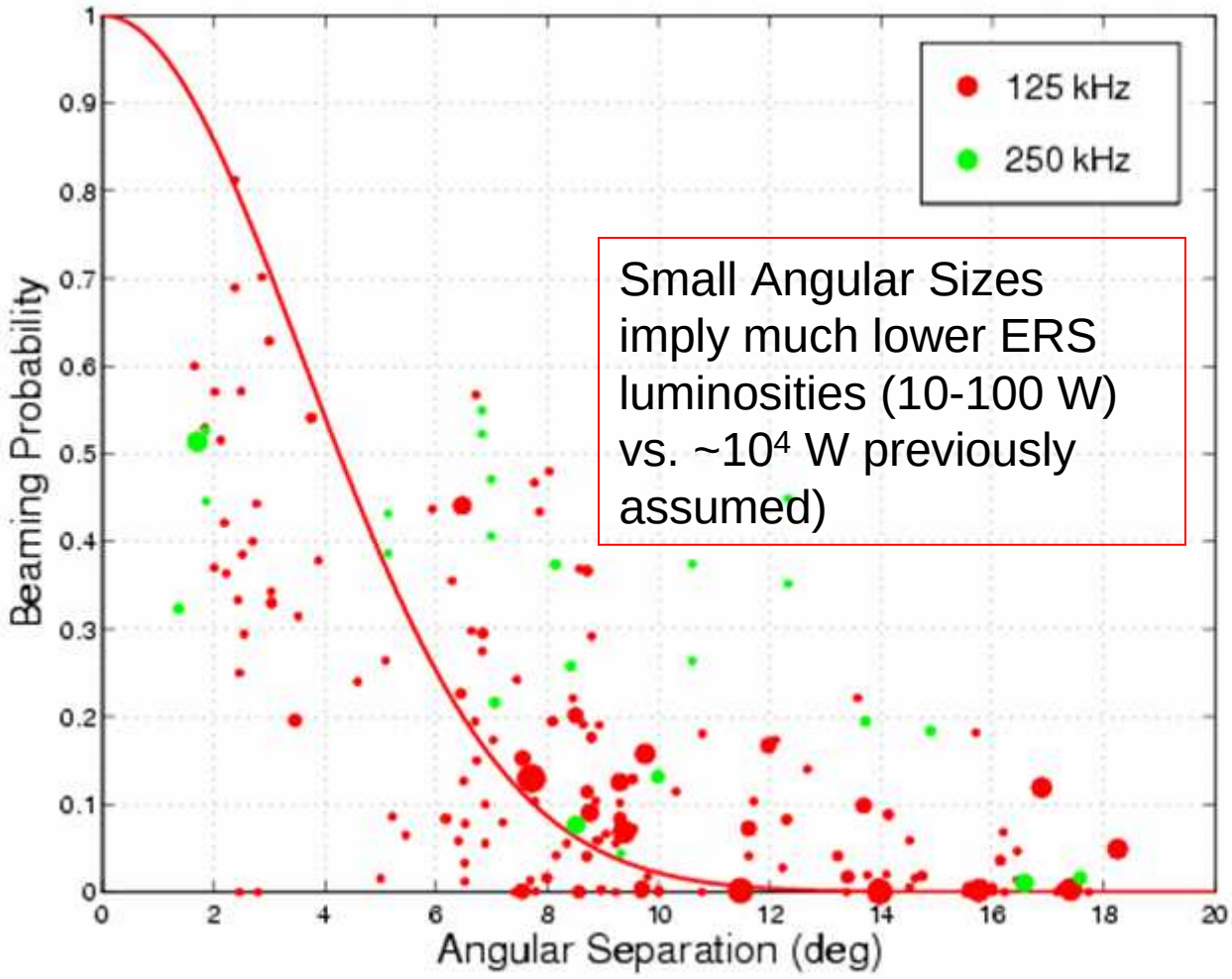

Figure xxx. Beaming probability of striated elementary AKR bursts measured at 125 kHz (red dots) and 250 kHz (green dots) bands using simultaneous observations of bursts at multiple spacecraft. The size of each dot is proportional the number of bursts measured. The solid line is a best-fit Gaussian function with half-maximum angular size $\theta = 4.2^{\circ}$.

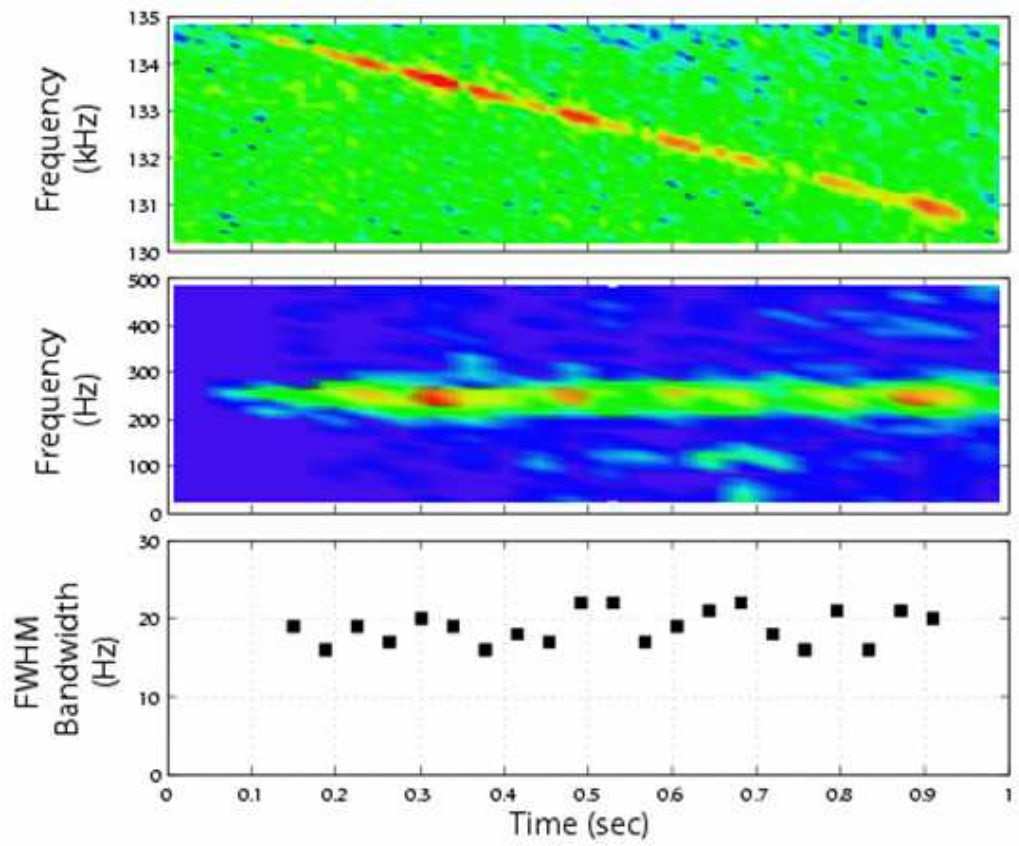

Figure xxx. (a) Isolated striated AKR burst dynamical spectrum observed on July 7, 2002 at 06:53:42 UT in the 125-137.6 kHz band. (b) De-trended burst dynamical spectrum computed by multiplying (heterodyning) the raw waveform with a chirp signal (constant df/dt) using the same frequency drift rate as the striated burst in (a), but with a small frequency offset (250 Hz). (c) Measured full-width at half-maximum (FWHM) bandwidth measured by fitting a Gaussian function to the one-dimensional frequency profile of each 37 ms time slice.

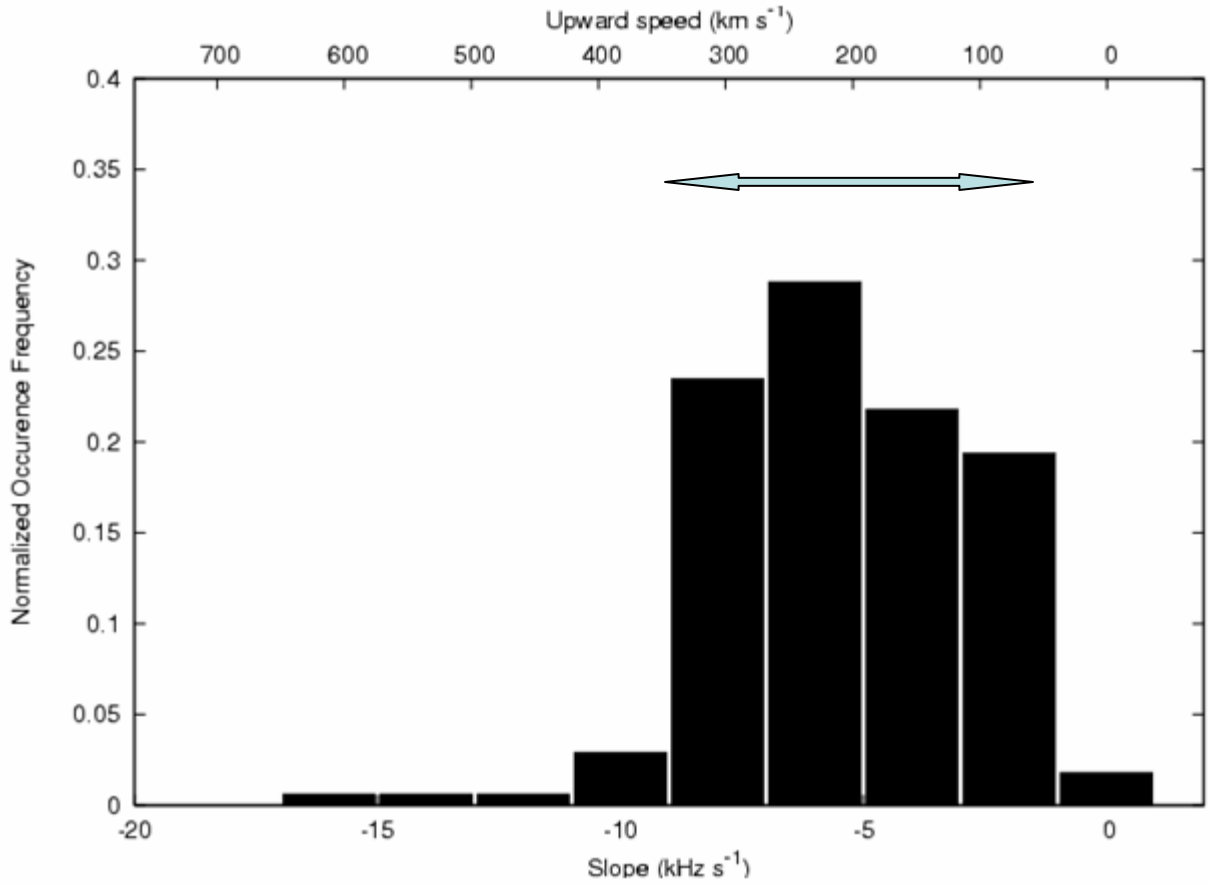

Figure xx. Striated AKR burst drift rate frequency of occurrence in the 125-135 kHz band based on observations of 573 striated AKR burst events. The mean slope at this band ,*df/dt* = -5.0 ± 2.0 kHz s^{-1}, is very similar to the mean slope -5.7±1.8 kHz s^{-1} observed in the 125 kHz -215 kHz band by *Menietti et al.* 2000. The upper horizontal axis indicates the corresponding upward speed of a disturbance which would trigger emission at electron cyclotron frequency f_{ce} = 130 kHz.

Summary of SAKR Properties and Implied properties of trigger

Observed SAKR Property	Implied Trigger Property	
Negative slope	Upward traveling	
Slope -3 → -12 km/s	Speed 75 – 300 km/s	
Narrowband (20 - 40 Hz)	Spatial scale < 1 km (along B field)	
Much more common at low frequency (100 KHz vs. 500 KHz	Trigger more common at higher altitude (R > 2.5Re)	
High intensity (comparable with normal AKR	E field must disturb electron f(v) significantly (for max. growth)	

Ion and Electron Solitary Structures (Bounds et al. 1999 JGR)

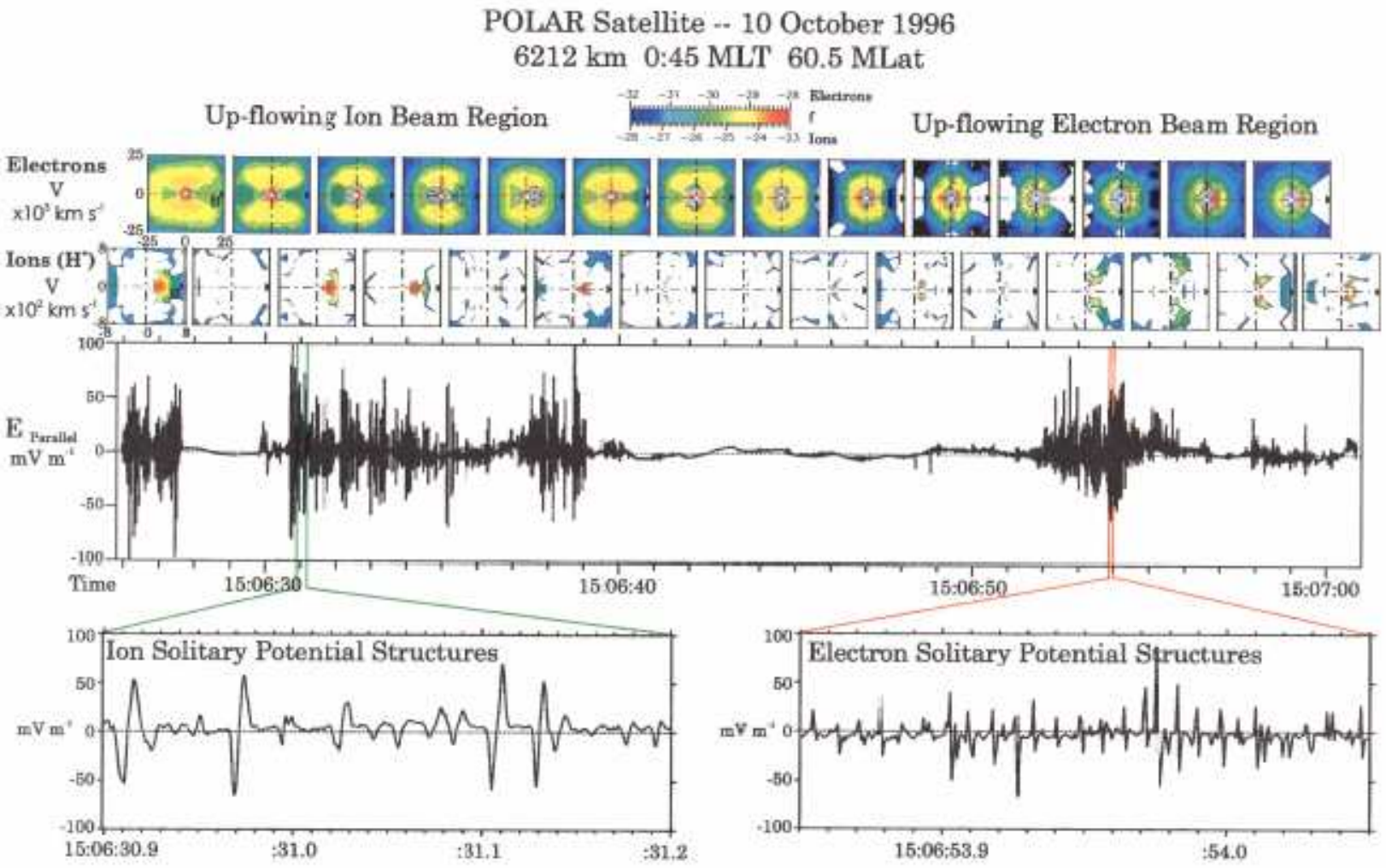

Plate 2. Time evolution of the ion and electron particle distributions with respect to contiguous observations of the parallel electric fields which include ion and electron solitary potential structures on October 10, 1996. The strong correlation of solitary potential structures and upflowing ion beams can clearly be seen in the first half of the data. In the ion solitary potential structure region, electrons display a loss cone type distribution and the ions display a strong anti-earthward parallel acceleration. The second half shows the distributions in a region of electron solitary potential structures. Here the total electron population is colder and does not show distinct loss cone features, whereas the ions show conic distributions. The electrons show anti-earthward directed beams accelerated parallel to the magnetic field.

Ion solitary structures move up B field at V ~75 - 300 km/s (Bounds et al. 1999)

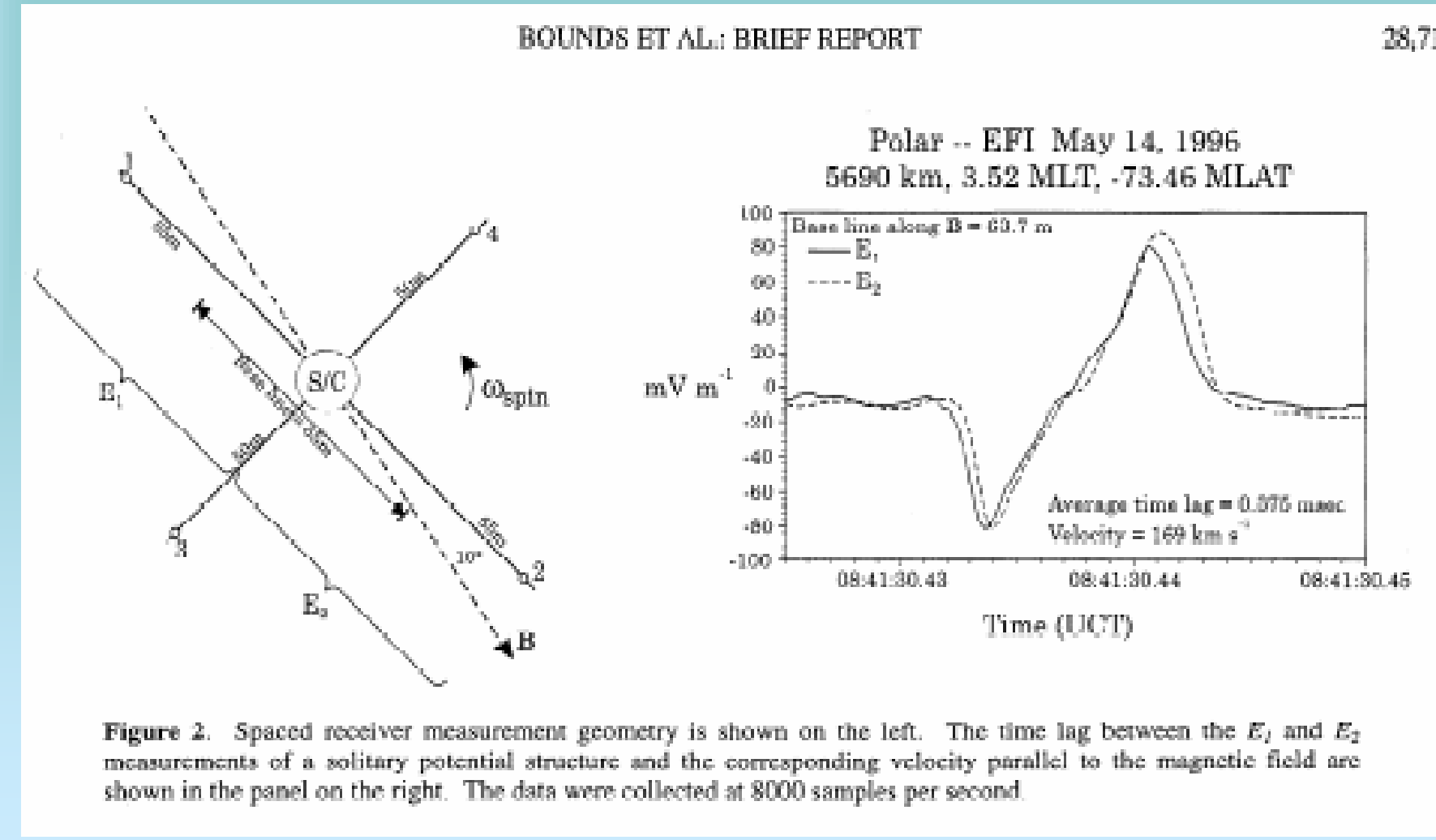

Figure 2. Spaced receiver measurement geometry is shown on the left. The time lag between the E_1 and E_2 measurements of a solitary potential structure and the corresponding velocity parallel to the magnetic field are shown in the panel on the right. The data were collected at 8000 samples per second.

Dipolar and Tripolar structures seen by Cluster 4.5 -6.5 R_e (Pickett et al. 2004)

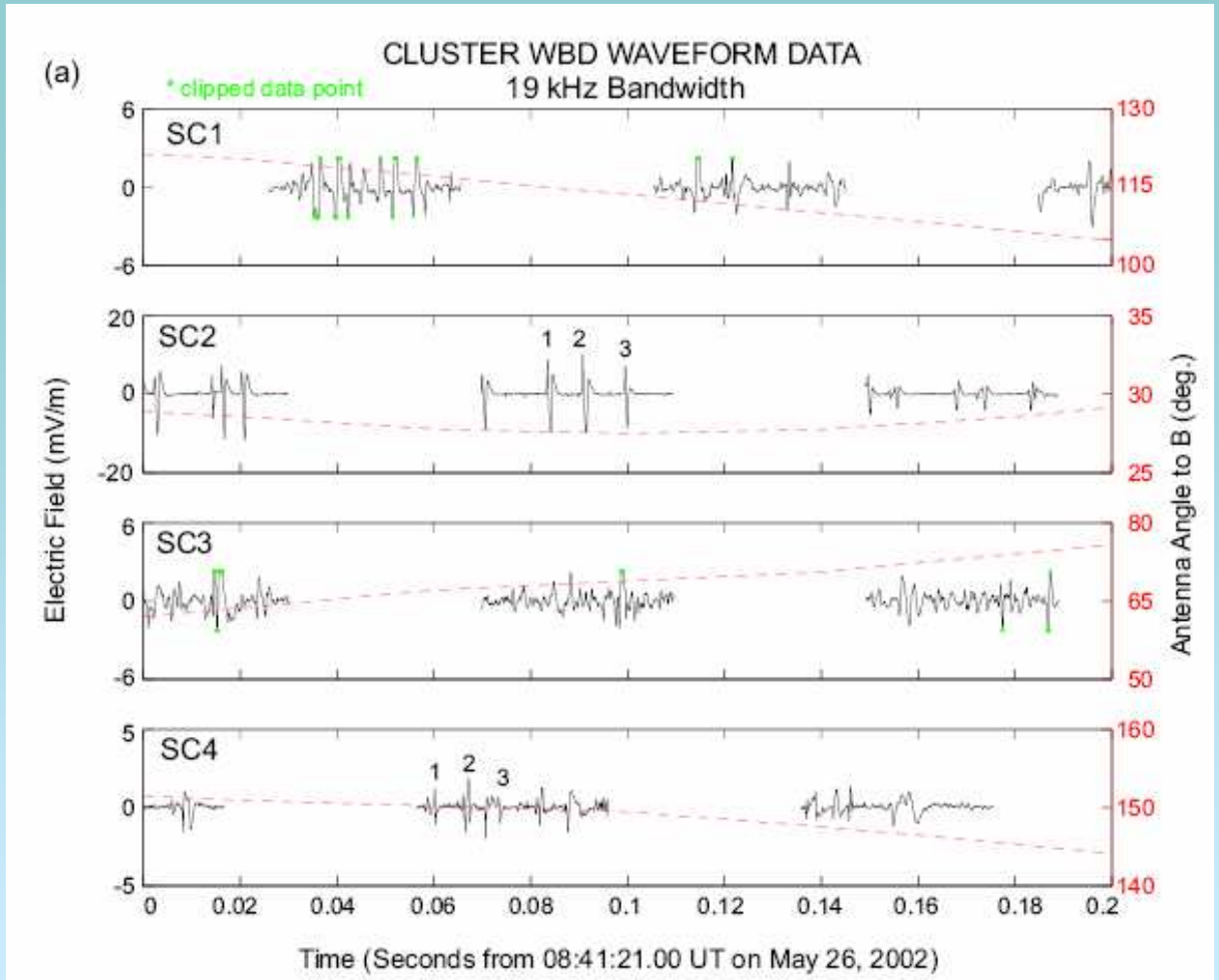

Velocity of tri-polar structure from Cluster SC lags

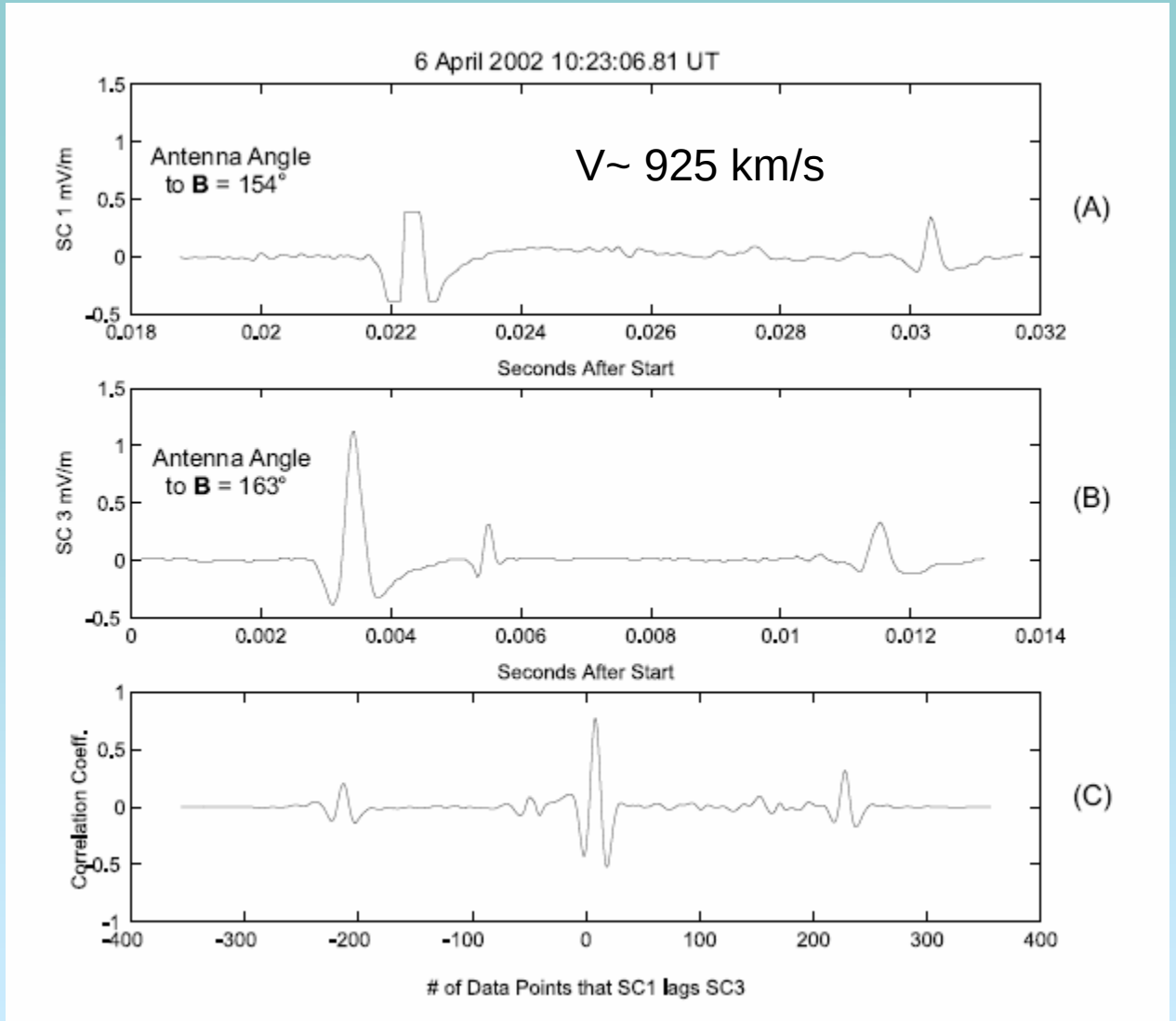

Ion hole and tri-polar solitary structures: Consistent with narrow bandwidths

$$\Delta t \approx 10\ ms$$

$$V_{ia} \approx 100 - 300\ km\ s^{-1}$$

$$L_z \approx 3\ km$$

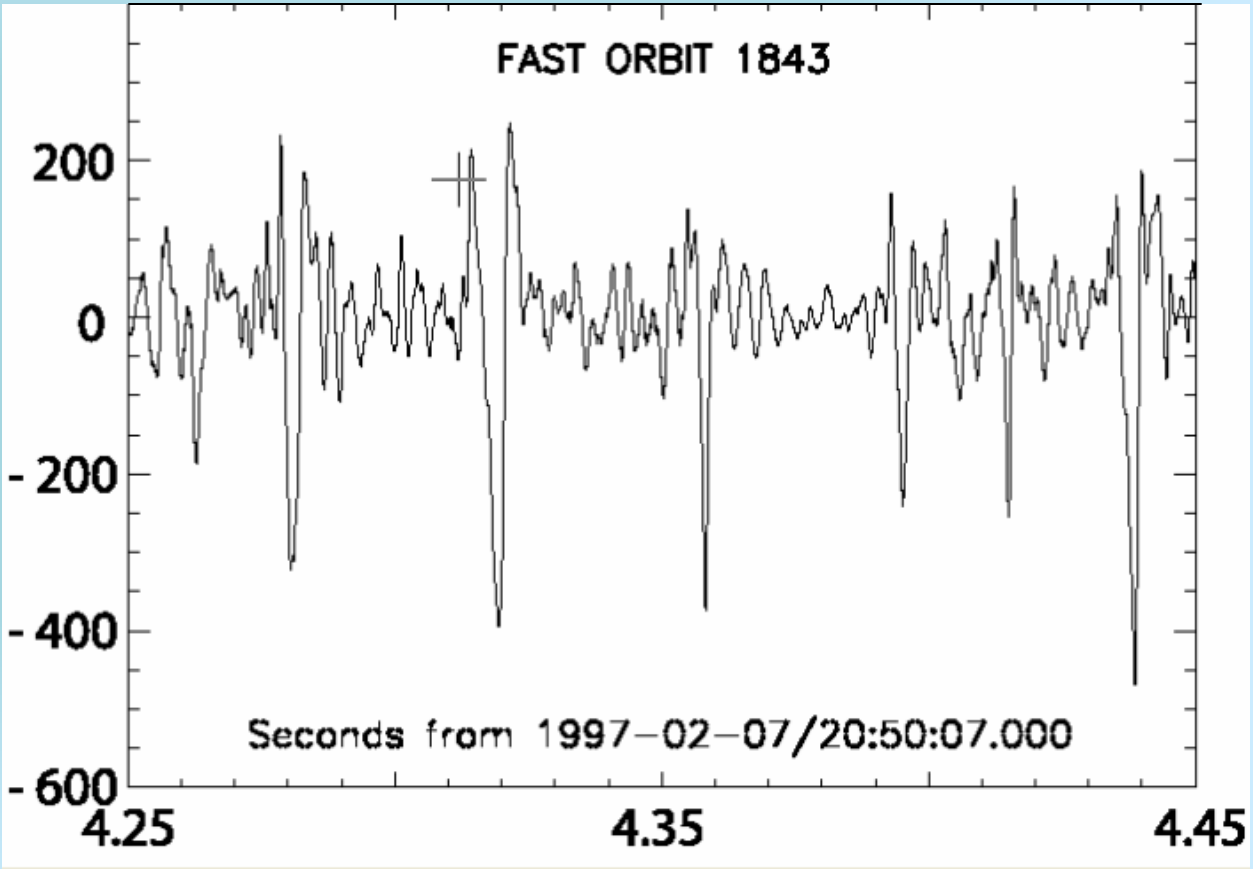

Bandwidths in excellent agreement

$$\frac{\delta\omega_B}{\omega_B} = \frac{\delta B}{B} = -3 \cdot \frac{\delta r}{r} \approx 2 \cdot 10^{-4}$$

Observed :

$$\frac{\delta\omega_B}{\omega_B} \approx \frac{0.02}{125} = 1.6 \cdot 10^{-4}$$

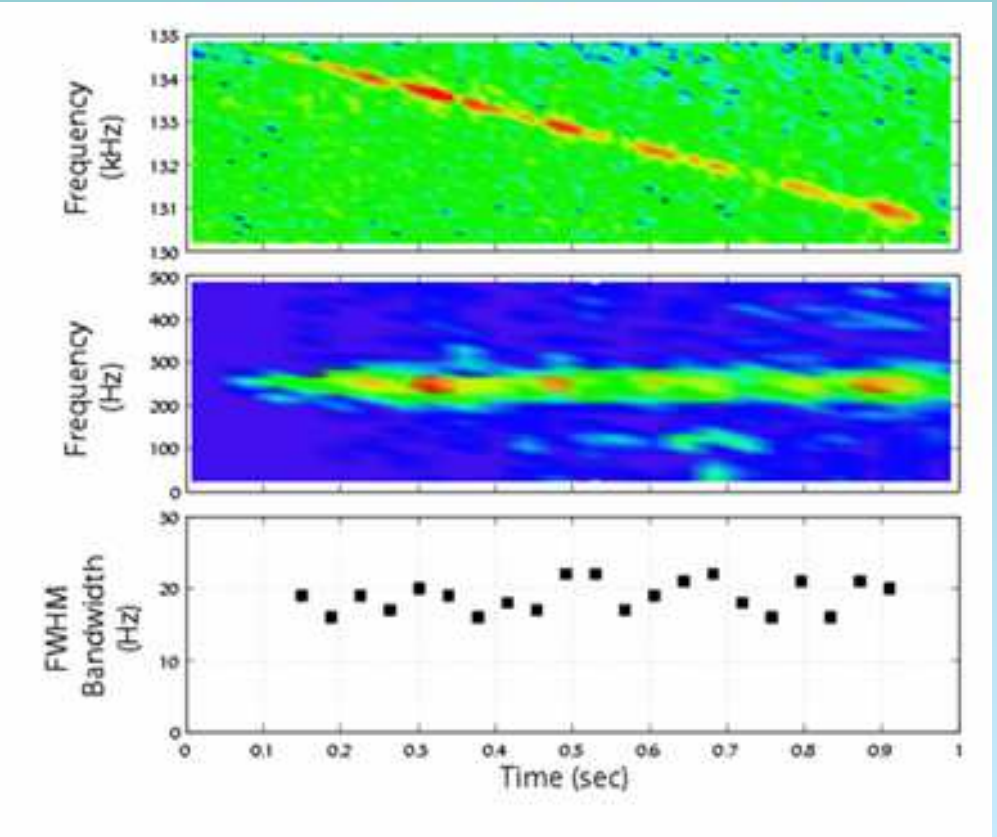

Ion holes: trigger for striated AKR bursts?

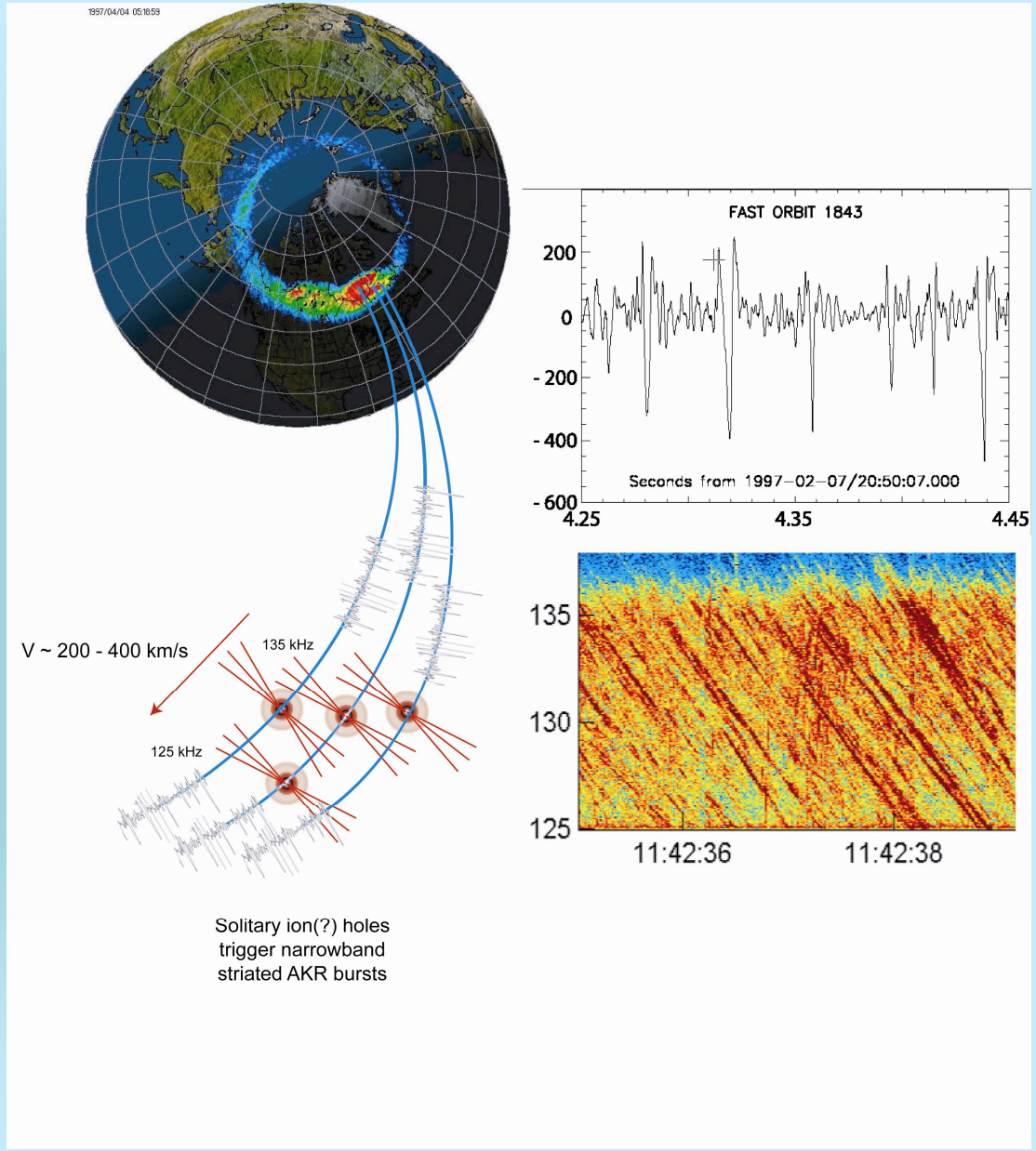

Electron-Cyclotron Maser (ECM) Resonance condition

$$k_{\parallel} v_{\parallel} - \omega + n\omega_{ce} = 0$$

$$\omega_{ce} \to \frac{\omega_{ce}}{\gamma}, \quad \gamma = \left(1 - \frac{v^2}{c^2}\right)^{-\frac{1}{2}} \approx 1 + \frac{1}{2}\frac{v^2}{c^2}$$

$$k_{\parallel} v_{\parallel} - \omega + n\omega_{ce}\left[1 - \frac{\left(v_{\parallel}^2 + v_{\perp}^2\right)}{2c^2}\right] = 0$$

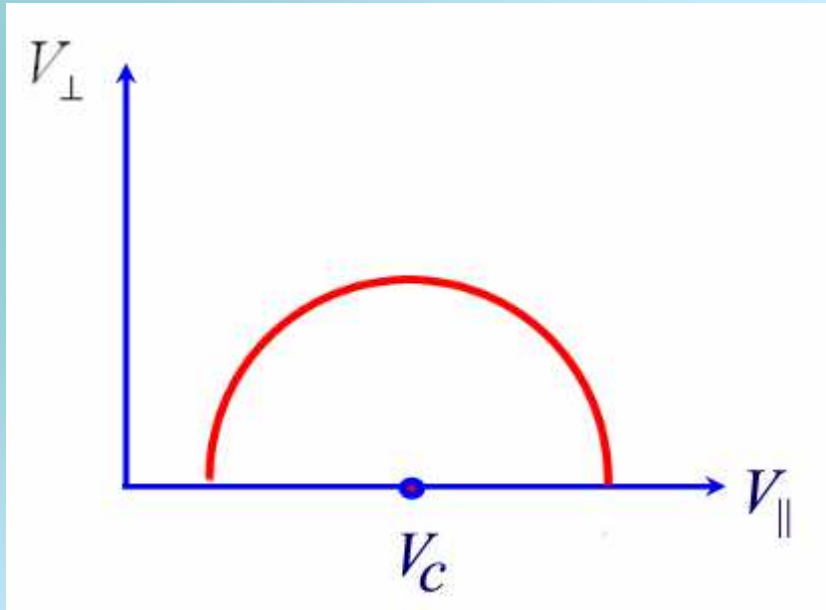

Electron energy dist function ('horseshoe') in magnetospheric acceleration region (Polar *in situ* obs)

$$\frac{\partial f}{\partial V_\perp} > 0$$

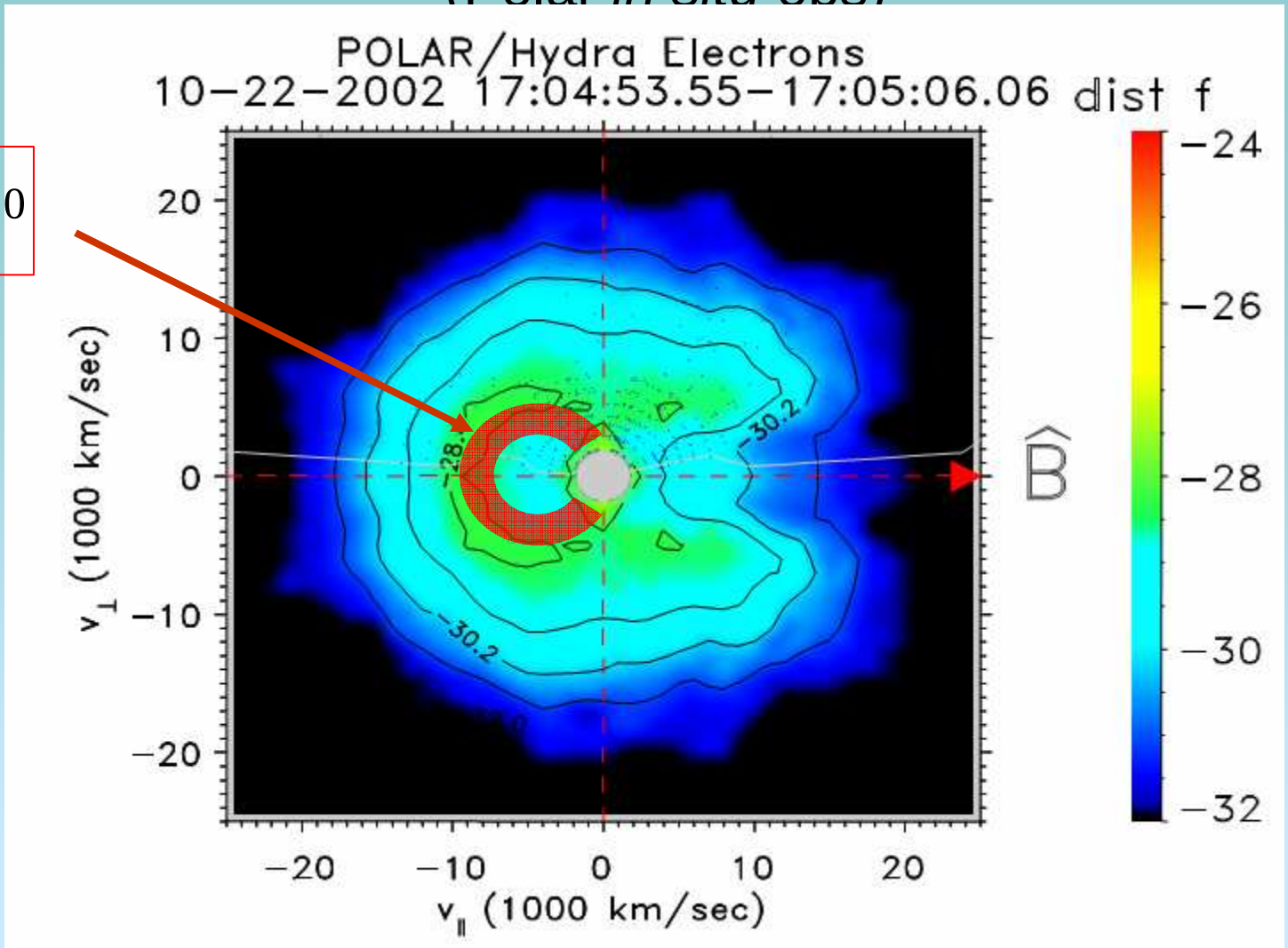

SAKR: A Tracer of Ion Solitary Structures?

Observed SAKR Property	Implied Trigger Property	Ion Solitary Structures
Negative slope	Upward traveling	Yes
Slope -3 → -12 km/s	Speed 75 – 300 km/s	Yes (e.g. Bounds, 1999)
Narrowband (20 - 40 Hz)	Spatial scale < 1 km (along B field)	Yes (many refs)
Much more common at low frequency (100 KHz vs. 500 KHz	Trigger more common at higher altitude (R > 2.5Re)	Unknown (but FAST measures in situ)
High intensity (comparable with normal AKR	E field must disturb electron f(v) significantly (for max. growth)	dE/dx ~ 0.5 V/m, V_{tot} ~ 0.1 kV. Requires detailed PIC code to verify

Summary

- Preliminary joint AKR (Cluster WBD VLBI) imaging with aurora (IMAGE) shows some correlation (but not high)
  - Is electron current return inefficient?
  - Ongoing joint observations started June 05 should clarify connection
- Striated AKR may be triggered by ion ‘holes’ (solitary structures)
  - Most observed parameters consistent with ion holes
  - Detailed PIC calculation, analytic integration of growth rate needed for verify